ABSTRACT

Title of Thesis: INVESTIGATIONS OF SUPERCONDUCTING FLUCTUATIONS THROUGH BROADBAND MICROWAVE CONDUCTIVITY EXPERIMENTS

Degree candidate: Hans Georg Breunig

Degree and year: Master of Science, 2000

Thesis directed by: Professor Steven M. Anlage

Department of Physics

The finite frequency conductivity of thin $YBa_2Cu_3O_{7-\delta}$ (YBCO) films has been studied at temperatures around the superconducting transition. The conductivity was measured using a special reflection technique in the continuos microwave frequency range from 45MHz-45GHz. The measurements were done, without an applied magnetic field, to investigate fluctuation effects in the region of the superconducting transition.

The measurements clearly show critical behavior in the frequency and temperature dependent complex conductivity above and below the superconducting transition temperature. The analysis of the frequency dependent data yields the dynamical critical exponent z and the critical exponent ν. Utilizing these derived values, it was found that it is possible to collapse the frequency as well as the temperature dependent data onto two universal curves. Such a data collapse was found for temperatures above and below T_C in the critical region using in both cases the same values for the critical exponents.

The value for the dynamical critical exponent z was found to be z=2.4-2.8 and ν=1.5-3.5, leading to a fluctuation lifetime τ^{fl} that diverges faster in the critical region than the prediction derived from Gaussian fluctuation theory.

INVESTIGATIONS OF SUPERCONDUCTING FLUCTUATIONS THROUGH BROADBAND MICROWAVE CONDUCTIVITY EXPERIMENTS

by

Hans Georg Breunig

Thesis submitted to the Faculty of the Graduate School of the
University of Maryland, College Park in partial fulfillment
of the requirements for the degree of
Master of Science
2000

Advisory Committee:
Professor Steven M. Anlage, Chair
Professor Richard L. Greene
Professor Christopher Lobb

Acknowledgements

A little more than two years ago, I came to the University of Maryland at College Park as an exchange student from the University of Bremen in Germany. Initially I planed to stay for only one year, but I changed my mind during that time.

I have been very lucky to have had Professor Steven Anlage as my thesis advisor. He gave me the opportunity to work in a very active group on an interesting project. Professor Anlage always stays in close touch with his group; discussions with him of all aspects of the experiment, the problems, and the achievements have been very helpful and fruitful for me. I would like to acknowledge him for directing me through all phases of this study. With his help I was not only able to finish this work successfully, but also to clear up bureaucratic problems that otherwise would have made this impossible.

I would also like to thank the members of my advisory committee, Professor Rick Greene and Professor Chris Lobb.

I have been working on this project closely with Andrew Schwartz. Andy not only introduced me to the experiment but to the work of an experimental physicist. He actively helped me in all stages of this work. He taught me how to attack experimental problems and especially to be patient if things initially do not work the way they are supposed to.

Furthermore I would like to thank the other members of Professor Anlage`s group: David Steinhauer, with whom I shared the lab, Lucia Mercaldo, Vladimir Talanov, David Kokales, John Lee, Atif Imtiaz, Kenton Brown and Ashfaq Thanawalla.

I would like to acknowledge all the people in the Center for Superconductivity Research who enabled me to work on this project. In particular I want to thank Patrick Fournier and Douglas Strachan for supplying me with samples for my measurement. Doug not only made the sample with which I obtained the data that are presented in this work, but provided me with many helpful discussions. He also showed me how to investigate the scaling behavior of the data effectively.

Finally, I would like to thank my family and my friends, in particular Jan Plath for lending me his laptop. The support and accompaniment of my girlfriend Ching-yi Hung has been very important to me. I am most grateful to her.

TABLE OF CONTENTS

LIST OF FIGURES

Chapter 1: Introduction

Every second-order phase transition, like the superconducting transition, is typically dominated by fluctuation effects. However, the critical region of conventional low temperature superconductors is so small that fluctuations usually do not affect the properties of the material very strongly.

With the discovery of the high-T_C oxide superconductors new materials became available, in which fluctuations play a more important role and affect their properties over a much larger temperature range. Although this discovery was several years ago [1], the nature of the transition in the high T_C superconductors is still not clear and its characterization is the focus of many experimental as well as theoretical investigations.

Fluctuations lead to the formation of superconducting regions inside the superconducting material even above its transition temperature T_C. Fluctuations affect the properties of the material also below T_C: normal-conducting regions can appear for short times in an otherwise completely superconducting system.

The effects of fluctuations are of manifold nature. Simply speaking one could say that fluctuations "round off" the superconducting transition. Because of them, there are no real discontinuities or sharp peaks in the temperature-dependent properties of the superconductor that otherwise would be expected to

emerge at T_C. Without fluctuations, the resistivity of a superconducting sample for instance would really drop instantly to zero at the transition temperature (T_C) and would be non-zero at any higher temperature, no matter how close to T_C that temperature might be. Another example is the temperature dependence of the heat capacity that would also have a sharp step at T_C in a system without any fluctuations at all.

These are only two instances but in fact, fluctuations manifest themselves in a number of ways. Naturally, they are most directly observed in transport or thermodynamic properties: Heat capacity, diamagnetic susceptibility or dc as well as ac-conductivity are typical examples.

Since the superconducting transition is a true phase transition, it can be characterized by critical exponents. These critical exponents are universal in the sense that they are independent of the individual quantity in which they are observed. They are also independent of the specific system that undergoes the phase transition. However, in the high-T_C materials observations of these properties have yielded a wide range of sometimes contradictory results.

The values of the universal critical exponents that characterize the transition differ between heat capacity measurements [2], observations of the microwave penetration length [3] , temperature-dependent dc-conductivity measurements [4], or the analysis of nonlinear current voltage characteristics

near T_C [5]. Recent measurements of the specific heat of $YBa_2Cu_3O_7$ samples even suggest that the critical exponents are asymmetric around T_C [6], which cannot be explained at all within the theory of a regular second-order phase-transition.

In this work fluctuation effects in the complex frequency- and temperature-dependent conductivity are investigated. The measurement we have done is a microwave reflection experiment employing a special configuration that directly yields the surface impedance of the sample. That data is then used to extract the complex frequency-dependent conductivity of superconducting films in the broadband microwave range 45MHz-45GHz.

The analysis of the data yields the critical exponents ν and z of the superconducting transition. In addition, the scaling behavior of the fluctuation conductivity above as well as below T_C is investigated. This continues the work of Jim Booth who made measurements with $YBa_2Cu_3O_7$ (YBCO) thin films and analyzed the data mainly above T_C [7,8].

The data presented here was obtained by measurements of YBCO thin films. During the time I have spent in the group of Professor Anlage I have also worked on measurements of $Pr_{1.85}Ce_{0.15}CuO_4$ (PCCO) films. PCCO belongs to the copper-oxide high-T_C materials; its transition temperature (~20K) is much lower than that of YBCO (~90K), which makes the measurement more difficult.

In order to reach these much lower temperatures required for measurements on PCCO, the existing experimental set up [9] had to be modified significantly. The changes include the use of a different material for the microwave coaxial cable connector (stainless steel instead of copper), effectively heat-sinking the cable and determining the sample temperature more accurately. Another modification is a small spring that provides a restoring force on the center pin that is essential to keep good electrical contact between the conductors of the cable and the sample. These changes have made the measurement technique very reliable and helped to improve the temperature stability. A more detailed description of the changes is given in chapter 4. The system is now capable of successfully making low-temperature measurements, unfortunately it still does not reach temperatures far below the transition temperature of PCCO, which are necessary for the data correction.

Chapter 2: Principle of the measurement

In the following, the principle of the measurement is introduced. This includes a description of its strengths and weaknesses and an explanation of what is actually measured. More detailed descriptions of the measurement method, the necessary correction procedures and the analysis of the data are given in chapters 4,5 and 8.

Our experiment makes use of a special broadband microwave reflection-technique with a configuration in which the sample forms an electrical short at the end of a coaxial cable. The coaxial cable is used as a microwave transmission line and guides the microwave signal to the sample. This method allows it to measure directly the complex surface impedance Z_S of the sample, which can be related to the complex conductivity σ ($\sigma=\sigma_1-i\sigma_2$) of the film. The measurement yields the real and imaginary parts of σ as a function of frequency in the broadband microwave range 45MHz-45GHz, as well as their temperature dependence.

Other methods to measure the complex surface impedance often make use of resonant techniques. In these cases, either the sample itself forms a resonant cavity or it is located inside a resonant cavity. The characteristics of the resonant system (resonance frequency, quality factor) can then be measured and

related to the properties of the sample. These methods usually have a very high precision; however they are limited to certain frequencies or to a very small range of frequencies around the resonance frequency. In contrast, broadband methods allow for measurements of the frequency dependence of Z_S over a wide range, although at the price of lower sensitivity.

It is also advantageous to investigate the effects of thermal fluctuations with frequency dependent measurements, because they lead to less ambiguity in the analysis of the data and provide information about the time dependence of the system under study. An example of an important part of the data analysis that makes use of the frequency dependence is the unique determination of the transition temperature by studying isotherms of the conductivity (see chapter 8).

Chapter 3: Surface Impedance

This chapter describes in some detail how the surface impedance Z_s of the sample is obtained. As mentioned before the experiment is a microwave reflection measurement: Microwaves are guided to the sample by a coaxial cable and reflected back. The reflected signal propagates back through the same coaxial cable and contains information about properties of the sample. The reflection coefficient S_{11} is measured using a network. S_{11} is the ratio of reflected (V_{ref}) and incident voltage (V_{inc}) signal in the transmission line:

$$S_{11} = \frac{V_{ref}}{V_{inc}} \qquad (1)$$

One should keep in mind that the analysis of the reflectivity described here assumes that the system is properly calibrated. A description of the calibration procedure and further corrections (temperature-related changes, background correction) is given in chapter 5.

Several steps are required in order to interpret the measured reflectivity signal and relate it to properties of the sample. Almost directly we can get the surface impedance Z_s, a physical quantity that provides relevant information in many different fields of condensed matter physics. The surface impedance is an interesting quantity for our measurement because it can be used to extract the

complex conductivity σ of the film. Once σ is obtained, it gives insight into the nature of the phase transition and fluctuations effects.

The analysis of the reflectivity data starts by using the fact that the S_{11}-signal can be related to the load impedance Z_{load} at the end of the transmission line by the following formula:

$$S_{11} = \frac{Z_{load} - Z_0}{Z_{load} + Z_0} \qquad (2)$$

where Z_0 is the characteristic impedance of the specific transmission line that is used in the measurement. In our case Z_0 is real and equal to 50Ω (i.e. $Z_0=(50+0i)\Omega$). The load impedance is the ratio of the total voltage across the Corbino disc to the total current flowing through the disc, i.e. $Z_{load}=V_{total}/I_{total}$ [1]. As can be seen from equation (2) S_{11} is in general a complex and dimensionless quantity with a magnitude bounded between zero and one.

The coaxial cable supports only the TEM mode, which is characterized by transverse electrical and magnetic fields. The TEM mode has no cut off frequency, this makes it in principle possible to make frequency dependent measurements down to the dc limit. In this case, the load impedance is proportional to the surface impedance Z_s of the sample. Hence:

$$Z_{load}=\Gamma Z_S \qquad (3)$$

The proportionality factor Γ is a geometrical factor. For coaxial cables $\Gamma=2\pi\ln(b/a)$, where a and b are the inner and outer radii of the coaxial cable.

The surface impedance Z_S is by definition equal to the field impedance Z_{field} at the surface of the sample, (i.e. $Z_S \equiv Z_{field}\big|_{surface}$). $Z_{field}=(E_r/H_\varphi)$ is the ratio of radial electric (E_r) and azimuthal magnetic field (H_φ). Z_S is the measurable quantity, which contains direct information about the electric properties of the sample like the microwave conductivity.

In the case were the sample is a thin film on a substrate, some part of the radiation will propagate through the thin film into the substrate. Therefore, the properties of the substrate will affect the signal so that substrate effects have to be taken into account in the analysis of the surface impedance-data.

The film and substrate act like a two-layer system for which it is possible to calculate an effective surface impedance Z_s^{eff}. For such a system, Z_s^{eff} depends on the impedances of the bulk sample (Z_{bulk}) and substrate material (Z_{sub}), the complex wavenumber k in the film and the film thickness t_0. Using an impedance transformation Z_s^{eff} can be calculated. Such an effective impedance is given by[2]:

$$Z_s^{eff} = Z_{bulk}\frac{Z_{sub} + Z_{bulk}\tanh(kt_0)}{Z_{bulk} + Z_{sub}\tanh(kt_0)} \qquad (4)$$

where Z_{bulk} is the surface impedance of a bulk sample of the material of the film (e.g. bulk piece of YBCO), Z_{sub} the impedance of the substrate and t_0 the film thickness.

The above equation (4) has two obvious limits: If there is no film at all (film thickness $t_0=0$) the effective impedance is equal to the substrate impedance ($Z_s^{eff}=Z_{sub}$). On the other hand, for a bulk material ($t_0\rightarrow\infty$) the equation recovers the impedance of the bulk material ($Z_s^{eff}=Z_{bulk}$). In the second case, the substrate does not contribute to the effective impedance, because no radiation penetrates through the first layer.

The expression for the impedance can also be significantly simplified in the intermediate region for metallic or metal-like samples in the case of the so-called thin-film limit. In this limit, the thickness t_0 of the film is much smaller than the skin depth δ (i.e. $t_0 \ll \delta$). To investigate the behavior of the effective impedance in this case it is useful to employ first the explicit formula for the impedance of the bulk material. The surface impedance of a metallic or superconducting copper oxide (in the normal state) bulk sample Z_{bulk} is given by:

$$Z_{bulk} = \sqrt{\frac{i\mu\omega}{\sigma}} \qquad (5)$$

depending on the frequency ω, the permeability μ and the conductivity σ of the material ($\sigma=1/\rho$), a quantity that is in general complex ($\sigma=\sigma_1-i\sigma_2$). The wave

number k of a metal is given by $k=(i\mu\omega/\rho)^{1/2}=(1+i)/\delta$, where $\delta=(2/\mu\omega\sigma)^{1/2}$ is the skin depth of a metal. In the thin-film limit $t_0 \ll \delta$ this is equivalent to $|kt_0| \ll 1$. The expression for the effective surface impedance can therefore be simplified by approximating the hyperbolic tangent function with its argument (i.e. $\tanh(kt_0) \approx kt_0$ for $|kt_0| \ll 1$). If this approximation is combined with the above expressions for Z_{bulk} (5) and k, the expression (4) for a thin metallic film on a substrate reduces to:

$$Z_s^{eff} \approx \frac{\rho/t_0}{1+\frac{\rho/t_0}{Z_{sub}}} \qquad (6)$$

This expression is also valid for copper-oxide superconductors above T_C.

Equation (6) makes it clear that substrate effects dominate Z_s^{eff} in the case the sheet resistance is much larger than the substrate impedance ($Z_s^{eff} \approx Z_{sub}$ for $\rho/t \gg Z_{sub}$). Substrate effects play an important role for Z_s^{eff} as long as $|\rho|/t$ is comparable to Z_{sub}, $\rho/t \approx Z_{sub}$. In the limit were $\rho/t \ll Z_{sub}$ the expression (6) for Z_s^{eff} further simplifies to:

$$Z_s^{eff} \approx \rho/t_0 \qquad (7)$$

The case where none, or only a very small portion, of the radiation penetrates through the film and any substrate effects can be neglected is realized, for example, for a superconducting film at temperatures far below T_C. That being

the case the wave number k reduces to $k \approx 1/\lambda$, where λ is the magnetic penetration length, whereas the expression of the effective surface impedance is the same provided that one defines the resistivity ρ as $\rho = \rho_1 + i\rho_2$, with $\rho_1 \approx 0$ and $\rho_2 = \mu\omega\lambda^2$ [3]. In other words the effective surface impedance Z_s^{eff} for a superconducting film below T_C is almost completely independent of the substrate and dominated by the kinetic inductance of the film: $Z_s^{eff} \approx i\mu_0\omega\lambda(T)^2/t_0$. Note that this impedance is enhanced by a factor of $\lambda(T)/t_0$ compared to the bulk value in the same limit.

Summing up, the directly measured reflectivity S_{11} of the sample can be related to the load impedance Z_{load}, which is related to an effective surface impedance of the film-substrate system. If the data are corrected for substrate effects (as described in section 5.2.2) and the film thickness t_0 is known, the effective surface impedance Z_s^{eff} yields directly the complex bulk resistivity ρ of a thin film sample. Having obtained ρ, the complex conductivity σ can easily be calculated. Both, ρ and σ are fundamentally interesting quantities, because they can be compared directly with theories that often give explicit expression for $\rho(T,\omega)$ or $\sigma(T,\omega)$.

Chapter 4: Experimental technique

4.1 General Overview of the set up

The objective of our measurement is to investigate fluctuations using finite frequency conductivity of superconducting thin films. The conductivity is obtained by measuring the surface impedance Z_s of the sample.

In the microwave range, this is often done by using resonance methods that allow very sensitive measurements of Z_s. However, these methods are necessarily limited to frequencies close to the resonance frequencies of the specific experimental system. To investigate the frequency dependence of the surface impedance a broadband technique is required that allows to measure Z_s continuously as a function of frequency.

The experiment described here is a microwave reflection measurement that yields Z_s of the sample in the broad frequency range 45MHz-45GHz. Using a network analyzer, the complex reflection coefficient S_{11} of the sample is measured. During the measurement, the sample forms an electrical short across the end of a coaxial cable. The coaxial cable is used to guide the microwaves from a microwave source to the sample and the reflected signal back to the network analyzer. The network analyzer calculates the reflection coefficient S_{11} by comparing incident and reflected signals. S_{11} can then be related to the surface

impedance of the sample using standard transmission line theory. In addition to the reflection coefficient, a two-point dc resistance between the inner and outer conductor of the coaxial cable can be measured simultaneously. For these measurements, a dc bias current is applied to the coaxial cable and the resulting voltage drop between the inner and outer conductor is measured. Measuring the dc resistance serves mainly as a check for the electrical contact between the sample and the coaxial cable.

A schematic overview of the set up is given in figure 1. The termination of the coaxial cable with the sample is located inside a continuos-flow cryostat

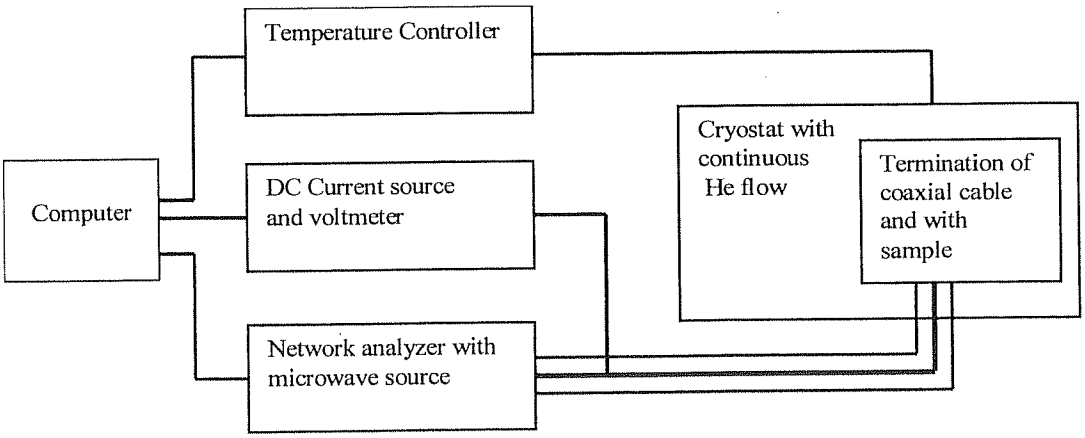

Figure 1: Schematic Overview of the experimental set up

(Janis model ST-100). The cryostat can be evacuated and cooled with liquid helium. The temperature is regulated by a temperature controller that uses a heater to ramp the temperature through the temperature range of the

measurement (Lakeshore temperature controller 340). During the measurement, the temperature changes by less then 2mK per minute. All measurement devices, the network analyzer, the dc current source with voltmeter and the temperature controller are connected to a computer that controls these devices and collects and saves the data.

The microwave source, a HP83651A synthesized sweeper, is part of the network analyzer system and provides microwaves in the range 45MHz-50GHz. During the measurement, it is operated in step mode with 201 frequency points. To ensure a constant power output at the termination of the coaxial cable at all frequencies, the frequency range is limited to 45MHz-45GHz. The power at the end of the coaxial cable is then adjusted to be –21.6dBm at all frequencies.

The measurement was performed with an existing apparatus that had been used before in several different measurements with different objectives. The apparatus was originally designed to study vortex dynamics [1], as well as the fluctuation conductivity in YBCO [2], but it has also been used to make surface impedance measurements in ferromagnetic materials (in particular $La_{0.8}Sr_{0.2}MnO_3$) [3].

To reach the lower temperatures required for making measurements in the vicinity of the phase transition of PCCO we modified the apparatus to heat sink the coaxial cable. Further modifications involve increasing the reliability (spring-

loaded center pin) of the system and a more accurate determination of the sample temperature by moving the temperature sensor to a position right behind the sample.

4.2 Corbino Geometry

The measurement takes advantage of a special geometry in which the sample is a thin disc forming an electrical contact between the inner and outer conductor. This geometry is referred to as the Corbino geometry.

The exact shape of the sample is not important, as long it is big enough to cover the outer diameter of the coaxial cable. The contact to the conductors of the coaxial cable is made through a modified V101F microwave connector. The modification makes it possible to press the sample directly against the inner and outer conductor while it is still possible to connect calibration standards to the connector. This is essential because before each measurement the system has to be calibrated at the same position where the sample is later mounted. A further description of the calibration is given in chapter 5.

The coaxial cable–sample interface is schematically shown in figure 2. The sample is firmly pressed against the termination of the cable by a spring-loaded copper pedestal. This copper pedestal slides inside a bigger cylindrical

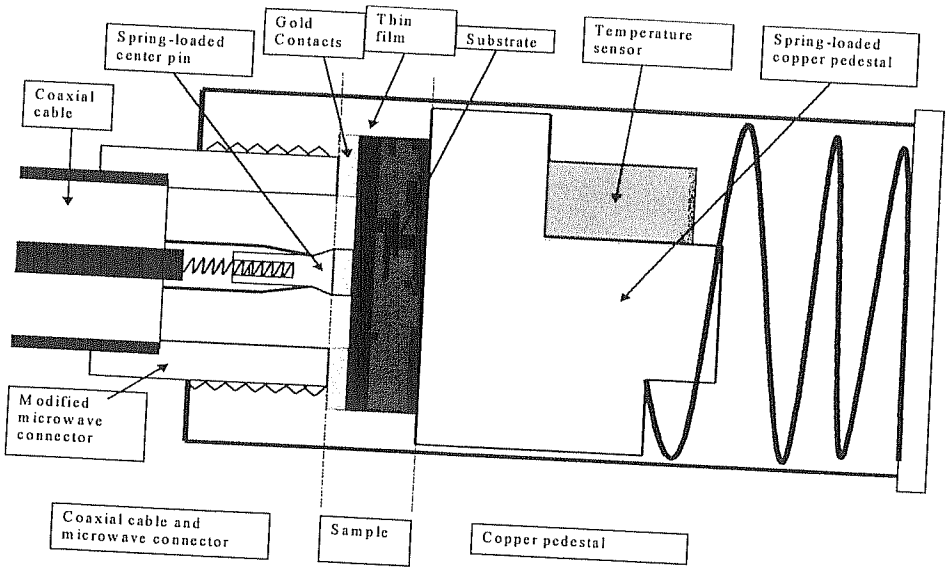

Figure 2: Schematic diagram of the cross section of the coaxial cable-sample interface

copper housing that is rigidly connected to the coaxial cable (screwed onto the connector).

It is important that there is always a good electrical contact (the lower the contact resistance the better) between the conductors of the coaxial cable and the sample. To improve this contact a thin layer of gold is evaporated through a mask on the film. The gold has a thickness of typically 1000Å. The mask has a shape of a ring such that the gold forms inner and outer conductors on the film. These contacts match the inner and outer conductor of the cable.

The electrical contact between sample and cable is made directly between the outer conductor and the film through the modified microwave connector. The contact between the inner conductor and the sample on the other hand is established by a center conductor pin, which is inserted into the connector center conductor. The pin is tapered down from a diameter of 0.020'' to 0.015''. This leads to a restoring force that presses the pin against the cable: While the thinner part slides inside the connector center conductor, the bigger top-part is pressed outwards against the sample. In addition, the pin is spring-loaded by a very small spring that is located inside the connector center conductor between center conductor and pin (see figure 2). The purpose of the spring is to provide an additional restoring force to ensure electrical contact is maintained between sample and inner conductor while the temperature is lowered. The dimensions of center pin and spring are crucial. If the diameter of the pin is much less then 0.020'' it slides too far inside the connector center conductor, if it is too large it perturbs the microwaves and resonances can occur making accurate frequency measurements impossible. The spring that goes inside the connector center and presses the pin out must be long enough to ensure that there is enough restoring force to press the pin out while lowering the temperature. At the same time, it must be short enough that the thinner part of the pin slides far enough into the center conductor. Such a contact can hold over the entire temperature range with changes in the contact resistance of usually less than 30mΩ during the cooling.

The springs that are used inside the center pin are very small. Originally, they were actually part of high-performance probe contacts (POGO-pins). They are employed inside a small barrel to provide a restoring force pressing the tip of the pin that slides inside the barrel. The POGO-pins we used here were made by the company Everett Charles Technologies (ECT) and have the model number MEPJ-22BD. By cutting the POGO-pins, the spring can be pulled out carefully with tweezers. The springs are initially too long for our purpose and have to be shortened to fit inside the Corbino-center-pin. Their inner diameter is approximately 0.0065", the outer approximately 0.0085". The Corbino-center-pins have a length of (0.060±0.005)", the hole inside is approximately 0.0045" deep and has a diameter of 0.009". The length of the spring has to be chosen in a way that it fits completely inside the hole of the center pin but sticks out a little bit when it is not compressed. If the spring is too long it deforms permanently and gets easily stuck inside the center pin. If it is too short it does not provide enough restoring force to the center pin and the electrical contact between pin and sample can be lost. We found that a spring of the type that is inside the POGO pin MEPJ-22BD must have a length of about 30 turns in order to function in the desired manner. 30 turns correspond to a length of approximately 0.01".

4.3 Measurement process

4.3.1 Overview

The experiment typically consists of two independent measurements over the same temperature range: In a first measurement we measure the actual sample, while afterwards in a second measurement the copper pedestal that usually holds the sample is measured alone. The second measurement is necessary to be able to correct for background contributions. The basic idea is that the conductivity of the copper changes very little over the measured temperature range. All changes in the signal of the background measurement can then be related to temperature dependent changes in the coaxial cable.

4.3.2 Preparation of the measurement

An important part of the preparation of each measurement is a calibration and the correct mounting of the sample on the copper pedestal in the position that gives the lowest contact resistance.

Before data can be taken, the system is cooled down very slowly (1-2K per minute typically) in order to avoid loss-of-contact-problems due to rapid thermal contraction. The cooling takes usually a few hours; the time for the data collection itself depends on the desired temperature stability of each

measurement and its range; in general, one complete frequency spectrum is measured every few minutes.

4.4 Sample Preparation

The samples studied in this work are several thousand Å thick $YBa_2Cu_3O_{7-\delta}$ (YBCO) films deposited on $NdGaO_3$ (NGO) single crystal 0.5mm thick substrates (5mm square typically) by pulsed laser deposition [4]. They were made by D. R. Strachan at the Center for Superconductivity research.

4.4.1 Thin film fabrication

The films we used in this study were grown by pulsed laser deposition. To do this, the $NdGaO_3$ substrate was attached to a heater plate using silver paste, which has a high thermal conductivity. First the silver paste is dried by heating the plate slowly to 100°C. Then the substrate and heater-assembly are loaded into a vacuum chamber, which is evacuated to $6*10^{-5}$ torr and heated to 825°C. Once the pressure is stabile, 146mtorr of oxygen is admitted into the chamber and the temperature is raised to the deposition temperature of 840°C. For the homogeneity of the sample it is important that the temperature is uniform within the substrate. The film is grown by hitting a $YBa_2Cu_3O_7$ target with laser pulses of 248nm at a rate of 10Hz. This leads the formation of plume of plasma above the surface of the target. By directing the plume towards the substrate, the

$YBa_2Cu_3O_7$ film is grown at a rate of roughly 3Å/s. The laser energy density is typically about 1.7J/cm^2. Once the desired film thickness is reached approximately 500 torr oxygen are admitted into the chamber and the film is annealed at 500°C for three hours and cooled back to room temperature.

The film used mainly for the measurements of this work is a 1500Å thick $YBa_2Cu_3O_{7+\delta}$ film with sample number ds67a. AC-susceptibility measurements give a transition temperature of T_C=87.6K. This is the temperature at the peak of the imaginary part of the ac-response. The transition width (i.e. 10% to 90% full width at half maximum) is approximately 0.8K

4.4.2 Gold contacts

As mentioned before the measurement depends crucially on good electrical contact between the sample and the modified microwave connector. To improve this contact gold contacts matching the shape of the connector are evaporated onto the film. This is done immediately after the film deposition. The films are taken out of the deposition chamber and mounted on a specially designed substrate holder. This holder has small magnets embedded into it. These magnets can hold a small shadow mask that is put on top of the film. The shadow mask itself is magnetic and therefore stays in place during the evaporation of the gold contacts. The gold is evaporated thermally forming inner and outer contacts on the film. The thickness of the gold layer is typically 1000Å. We found that it

is very important to try to minimize the time the film is exposed to air. With the procedure described above the time between taking the film out of the deposition chamber and putting it into the evaporator is not longer than 15 minutes.

Chapter 5: Calibration and error correction

5.1 Calibration

Before the start of each measurement, the system has to be calibrated. The calibration removes systematic errors and makes the measurement sensitive to the sample, which otherwise would only be a very small contribution to the total signal that is measured. It is performed at room temperature using calibration standards; since the measurements described here are made in a range of temperatures all much lower than room temperature, a second calibration procedure is done. Room and low temperature calibrations are described in the next two sections [1].

5.1.1 Calibration at room temperature

In an uncalibrated system, the measured reflection coefficient S_{11} is in general dominated by effects that are not caused by the sample. For our measurement, these effects can be seen as systematic errors. These include effects due to the coaxial cable, connectors, multiple reflections and systematic errors of the measurement hardware. A calibration removes these effects and makes the system sensitive to the plane where the calibration is performed.

All systematic errors that are removed by the calibration can be classified in three different categories and described by three complex error terms: E_R, E_D and E_S. These error terms depend on the frequency and characterize completely any effects of the transmission line or the detection apparatus to the measured signal.

The reflection tracking E_R corrects the change of the signal that propagates in the transmission line (including connectors). This change is described by a phase offset and attenuation in the line. The phase offset and attenuation depend on the actual length of the line and its particular phase constant β as well as the attenuation constant α. In general $\alpha \sim R_S$ and $\beta=\omega(\mu\varepsilon)^{0.5}$ depend on the material of the transmission line and are also frequency dependent ($\gamma=\alpha+i\beta$ is the propagation constant).

The error term E_D, the directivity, considers errors of the directional coupler inside the network analyzer and reflections due to the connectors of the system. Because of these effects, a small part of the signal from the source goes directly into the detector without being reflected off the sample.

E_S, the source match, describes the effect of single or multiple reflections of a part of a signal that is reflected back inside the network analyzer due to a small impedance mismatch between detectors.

The total effect of the calibration can be described in an equation that relates the measured S_{11}-signal, S_{11meas}, to the actual signal, $S_{11actual}$, coming from the sample (or whatever is at the position at which the system is calibrated)[1]:

$$S_{11meas} = E_D + \frac{E_R S_{11actual}}{1 - E_S S_{11actual}} \qquad (8)$$

The procedure to determine E_R, E_D and E_S consists of connecting calibration standards with known responses to the end of the transmission line. By comparing the measured response S_{11meas} of each standard to the known theoretical response at each frequency point, the network analyzer is able to compute E_R, E_D and E_S. It stores the error terms internally, and by inverting the above equation (9), calculates $S_{11actual}$ in all subsequent measurements. Hence, once E_R, E_D and E_S are known the $S_{11actual}$ is given by the relation:

$$S_{11actual} = \frac{S_{11meas} - E_D}{E_R + E_S S_{11meas} - E_D} \qquad (9)$$

$S_{11actual}$ is automatically determined during subsequent measurements by the network analyzer. The calibration standards that are used to determine the error terms are a perfect short, a perfect open, a 50Ω load (matches exactly the impedance of the transmission line) and a sliding load. During the calibration procedure, the reflection coefficients of these devices are measured for each frequency point in the same frequency range where the actual measurement is

later performed. To apply the calibration correctly to an actual measurement the sample has to be as close as possible to the location where the calibration was performed. The measurement described here makes use of a modified microwave connector to contact the sample. Hence, the calibrations are performed using the same modified connector that is directly at the location of the sample.

5.1.2 Calibration at lower temperatures

The calibration procedure described in section 3.1.1. is performed at room temperature. However, all microwave measurements with superconducting films were done at a range of temperatures all much lower than room temperature. This causes the following problem for the calibration: Since the sample is in direct contact with the transmission line, the temperature of at least a portion of the coaxial cable will also change. The electrical properties of the transmission line depend on the temperature; hence, the accuracy of the room temperature calibration is affected. The temperature changes have effects on the length of the transmission line, its dielectric constant ε as well as the surface resistance R_S of inner and outer conductor. Since $\beta \propto \varepsilon^{1/2}$ and $\alpha \propto R_S$ these changes change the propagation constant γ ($\gamma=\alpha+i\beta$) of the transmission line.

It can be reasonably assumed that not all three error-terms are affected in the same way by cooling of the sample. The directivity (E_D) and source match

(E_S) occur mainly due to effects inside the network analyzer, which is outside the cryostat and stays at room temperature. Therefore the cooling affects almost exclusively the third error term E_R, the reflection tracking.

The reflection tracking is caused by the whole transmission line, so it is possible to correct for any temperature-dependent changes by determining E_R at low temperatures. This is done by a further calibration procedure using the superconducting film itself as a reference. Far below the transition temperature, the film acts like a perfect short over the measured frequency range. A perfect short has the known reflectivity S_{11}^{short}=-1+0i. So a measurement of S_{11} at a temperature T_{low} far below the transition temperature can be used to recalculate E_R to get $E_R(T=T_{low})$ using the theoretical response (S_{11}^{short}) the measured response S_{11}^{meas} and the earlier measured values for the error coefficients E_D and E_S. Once $E_R(T_{low})$ is obtained it can be used to correct all S_{11} data in the measured temperature range $T_{low} \leq T \leq T_{high}$, were T_{high} is the highest temperature of the temperature ramp.

5.2 Error Correction

5.2.1 Background correction

Section 5.1.1. describes how the room-temperature calibration is corrected at lower temperatures using the sample itself at a temperature T_{low} as a further calibration standard. This allows to recalculate E_R to get $E_R(T_{low})$

However even with the recalculated $E_R(T_{low})$ the calibration will actually only be valid at the temperature $T=T_{low}$. A further correction is needed at each temperature $T>T_{low}$ of the measurement range to account for changes in the transmission line over that range. This background correction is done by measuring the response signal of the copper pedestal that supports the sample during the actual measurement. For that purpose the response of the copper block is measured at the same temperatures as the sample. With the assumption that the contributions of the copper itself to the S_{11}-signal do not change between T_{low} and T_{high}, all changes in the measured S_{11} signal are related to temperature dependent changes within the transmission line. The S_{11} data are corrected for these temperature dependent changes by directly subtracting off the changes $\Delta S_{11}=S_{11}(T)-S_{11}(T_{low})$ (in phase and magnitude) in the measured response of the copper pedestal.

Using the response of the sample at T_{low} as a reference also serves another purpose: The normal calibration is done using the commercially available calibration standards, which screw onto the (modified) microwave connector. The calibration obtained that way can only correct measurements that are done at exactly the same position. The sample on the other hand has a flat surface and is in contact with the inner conductor through a small center pin that slides into the connector center conductor. Since the calibration is performed without the pin, it will in general introduce new disturbances and errors in the measurements. The copper block used to determine background contributions to the measured S_{11}^{meas} is also flat and measured with the center pin in place. Hence using it as a further calibration standard to recalculate E_R also removes the effects on the signal due to the center pin.

5.2.2 Substrate Effects and their correction

As described in chapter 3 the measured S_{11} signal can be used to determine an effective surface impedance Z_s^{eff} of the two layer system substrate-film. In the thin-film limit ($|kt_0| \ll 1$) Z_s^{eff} is given by the equation:

$$Z_s^{eff} \approx \frac{\rho / t_0}{1 + \frac{\rho / t_0}{Z_{sub}}} \qquad (10)$$

Since we are interested in the properties of the film, hence in the complex sheet resistance ρ/t_0, the substrate will be a source of errors due to the transmission of radiation through the film and into the substrate, provided that the thickness of the film is sufficiently small. However even for thin films the effect of the substrate on the measured effective impedance Z_s^{eff} depends strongly on the temperature. In the limit were $|\rho|/t_0 \ll |Z_{sub}|$ the effects of the substrate are negligible. This limit is realized for superconducting films regardless of the thickness t_0 (sufficiently far) below T_C were $|\rho|$ is very small.

In order to correct for contributions of the substrate to Z_s^{eff}, Z_{sub} has to be measured. Once Z_{sub} is known, the above equation (10) can be inverted to extract ρ/t_0 as a function of the quantities Z_s^{eff}, which is measured as a function of frequency and Z_{sub}. By the substrate impedance Z_{sub} we actually mean here an effective substrate impedance including effects due to resonances inside the substrate. Therefore, Z_{sub} depends also on the specific geometry and orientation of the sample during the measurement, not only on the impedance of the material of the substrate. In order to determine Z_{sub} the sheet resistance $R_{square}=\rho_{dc}/t_0$ is determined independently at a temperature T_N, where the film is in the normal state. R_{square} is related to the measured two-point resistance R_{meas} between the inner and outer conductor of the Corbino disc:

$$R_{meas}=R_{square}\ \ln(b/a)/2\pi \qquad (11)$$

In the normal state the imaginary part of ρ is zero and the real part can be assumed to be frequency independent and therefore equal to the DC value of the sheet resistance $R_{sheet.}$ In other words: $\rho(T_N, f)/t_0 \equiv \rho_{DC}(T_N)/t_0$ [2]. If then the effective surface impedance Z_s^{eff} of the film-substrate system is measured at T_N, $Z_{sub}(T_N, f)$ can be calculated from the equation (10) for Z_s^{eff} since Z_s^{eff} and ρ/t_0 are known at T_N. Assuming further that the substrate impedance does not change with temperature over the measured temperature range, that is $Z_{sub}(T)=Z_{sub}(T_N)$ for $T_{low} \leq T \leq T_{high}$, $Z_{sub}(T_N)$ can be used in equation (10) together with the measured Z_s^{eff} to calculate $\rho(T,f)/t_0$ at temperatures T different from T_N.

The magnitude of the effective substrate impedance $|Z_s^{eff}(T_N,f)|$ at T_N=125K determined by the method described above is shown in figure 3.

The figure shows that $|Z_s^{eff}(T_N,f)|$ is very high at low frequencies and falls off roughly like 1/f. At a given temperature above the transition temperature substrate effects therefore have a greater influence at higher frequencies on the measurement.

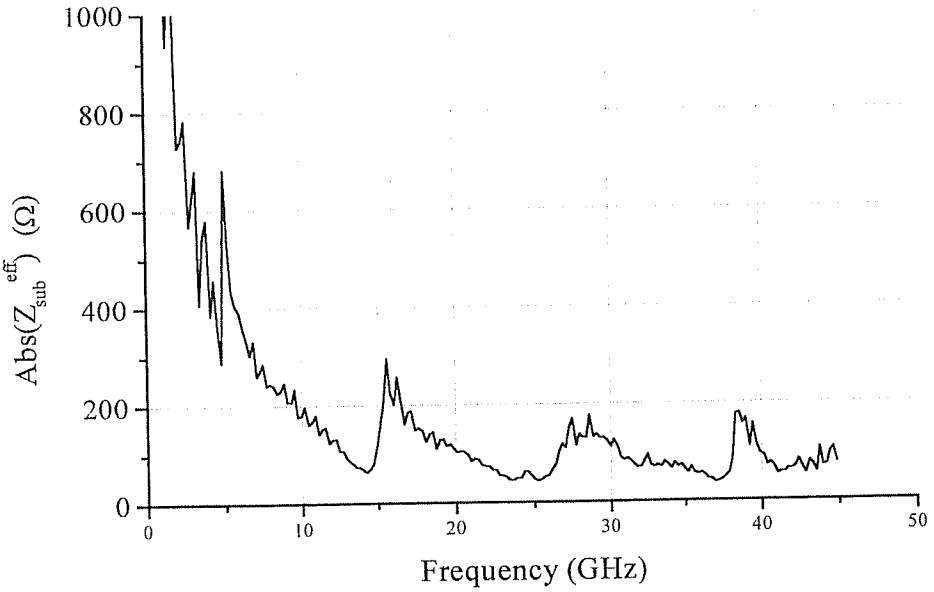

Figure 3: Magnitude of the effective substrate impedance versus frequency

Chapter 6: Fluctuation effects in the conductivity of superconductors

Fluctuation effects near phase transitions have been the focus of many investigations. These fluctuation effects typically dominate second order phase transitions including the superconducting phase transition.

However, the critical regime of low T_C superconductors is usually too small to measure critical behavior. This is a result of the low value of T_C as well as the large coherence length ξ in these materials. This limits fluctuations, because the energy required for the formation of a coherent volume is large and there is only little thermal energy available. Only in an unobservably small region close to T_C do the effects of critical fluctuations become significant [1].

Contributions due to fluctuation effects are supposed to be larger in high-T_C materials, where the transition temperature is higher and the coherence length shorter than in conventional superconductors. Fluctuation effects in these materials are not only stronger but the temperature range over which they are important is much wider. Their effects can be observed in a number of different thermodynamic and transport properties, like the specific heat, the diamagnetic susceptibility, dc conductivity and ac conductivity.

This chapter describes a systematic study of fluctuation effects in the temperature and frequency-dependent microwave conductivity of PCCO thin films near T_C. These fluctuation effects are important above as well as below T_C. Qualitatively, at temperatures above T_C fluctuations cause small regions of the sample to become briefly superconducting, although their surrounding remains normal. Similarly, below T_C, small regions of the superconducting material can become normal.

Fluctuations appear in samples of all dimensionality. Their importance, however, is not equal in all dimensions, but increases with reduced dimensionality. It is therefore favorable to study thin films rather than bulk material [2].

The size ξ and lifetime τ of the fluctuating regions depend on the temperature T of the system, and diverge as T approaches the transition temperature. This behavior, as well as the phenomenon of fluctuations in superconductors itself, can be described, for example, by the Ginzburg-Landau theory. A brief description of the Ginzburg-Landau theory is given in section (6.2.1). It leads to the Gaussian fluctuation theory that has been used to describe results of previous work [3]. However, Gaussian fluctuations do not describe critical fluctuations near T_C. In this region, the correlation length ξ and the fluctuation lifetime τ diverge differently from the Gaussian predictions.

With the Corbino reflection technique, it is possible to obtain the frequency dependence of the conductivity, in addition to the temperature dependence, so that the nature of the phase transition can be investigated in detail. By measuring the frequency dependence of the magnitude and phase of the fluctuation conductivity, the thermodynamic critical temperature T_C as well as the dynamical exponent z can be obtained. This would be more difficult with techniques that use only temperature dependence at specific frequencies.

Booth`s measurements [3] of the fluctuation conductivity in YBCO thin films revealed a value of z=2.3-3 and ν=1-1.5 indicating a critical region around the transition temperature in which the fluctuation lifetime diverges much more rapidly than predicted by Gaussian theory. Gaussian theory predicts ν=1/2 and is based on the assumption that z=2.

6.1 Fluctuations in Superconductors

The following is intended to give a brief description of the Ginzburg-Landau theory and introduces it only as far as it is necessary in this context. Mainly I want to define the Ginzburg-Landau coherence length ξ and relaxation time τ and explain their physical meaning as a description of the size and the lifetime of fluctuations. Extensive treatments of the Ginzburg-Landau theory can be found in many textbooks and publications [4,5,6].

6.1.1 Mean field theory

The Ginzburg-Landau theory is a mean field theory that uses a phenomenological approach to describe macroscopic properties of all types of superconducting materials. It can also be expanded to provide a description of fluctuation effects on thermodynamic properties, by employing small fluctuations around the mean-field solutions (Gaussian fluctuation theory). This leads, for example, to the formulas for the fluctuation conductivity described in section 6.1.1.2. However, if the fluctuations are not small, as in the critical region of the transition, the Gaussian fluctuation theory breaks down and a more general approach, which uses scaling theory, is necessary. A brief description of the more general scaling theory is given in chapter 7.

The Ginzburg-Landau theory describes the superconducting state by introducing a complex order parameter ψ. It is then postulated that $|\psi|$ is small so that an expansion of the free energy in terms of ψ can be performed. The coherence length ξ is a characteristic length that describes the spatial extent of the fluctuations. It can be written as:

$$\xi(T) = \xi(0)\,|\varepsilon|^{-0.5} \tag{12}$$

where

$$\varepsilon = \frac{T - T_C}{T_C}.$$

ξ_0 is a non universal length scale that depends on the specific sample.

That the order parameter ψ is not only small but also varies only slowly in space is a second basic assumption of the Ginzburg-Landau theory. With these assumption in place, the free energy density of the superconducting state relative to the normal state $\Delta f=f_{sc}-f_n$ can be expanded in a series:

$$\Delta f = \alpha|\psi^2| + \frac{\beta}{2}|\psi|^4 + \frac{1}{2m^*}\left|\left(\frac{\hbar}{i}\vec{\nabla} - e^*A\right)\psi\right|^2 + \frac{h^2}{8\pi} \qquad (13)$$

where $\alpha=\alpha_0\varepsilon$,with α_0 and β positive temperature-independent constants close to T_C.

For a spatially uniform order parameter minimizing Δf with respect to variations in ψ leads to the most probable value ψ_0:

$$|\psi| = \psi_0 = 0 \qquad \text{for } T > T_C$$

$$|\psi| = \psi_0 = (-\alpha/\beta)^{-0.5} \qquad \text{for } T < T_C$$

So the most probable value of the order parameter is zero above and nonzero below the transition, which is what one would expect if there were no fluctuations. However, above T_C other values of $|\psi|$ are also probable, as long as the values of the free energy F stay within k_BT of the minimum value ($F=\int \Delta f dV < kT$). That means that even above T_C superconducting effects can occur, leading for example to an increase in the conductivity of the normal state.

Below T_C there are also fluctuations in the order parameter leading to deviations of $|\psi|$ from its equilibrium value.

6.1.2 Fluctuations above T_C

To investigate fluctuations above T_C we reconsider the equation (13) for Δf. If the fluctuations above T_C are small, we can drop the term proportional to $|\psi|^4$. Note that this assumption is not valid in the critical region that is fluctuation dominated. This so-called Gaussian approximation leads to the following expression for the GL free energy density Δf_{Gauss} relative to the normal state:

$$\Delta f_{Gauss} = \alpha|\psi^2| + \frac{1}{2m^*}\left|\left(\frac{\hbar}{i}\vec{\nabla} - e^*\mathbf{A}\right)\psi\right|^2 \qquad (14)$$

A is here the vector potential, e^* and m^* are effective charge and mass.

In the following, I want to derive the Ginzburg-Landau coherence length ξ and explain its physical meaning. For that it is sufficient to consider the zero field case (**A**=0). In zero field it is appropriate to expand $\psi(r)$ in a Fourier series:

$$\psi(\mathbf{r}) = \sum_k \psi_k \exp(i\mathbf{k}\cdot\mathbf{r}) \qquad (15)$$

Putting this into the expression of the free energy density, we obtain for Δf_{Gauss}:

$$\Delta f_{Gauss} = \sum_k \left(\alpha|\psi^2| + \frac{\hbar^2 k^2}{2m^*}\right)|\psi|^2 \qquad (16)$$

A possibility to obtain an expression for the coherence length ξ is to compute the thermodynamic average of $|\psi|^2$ using the above expression (16). $|\psi|^2$ can be found by taking the direct thermodynamic average over all possible values of the order parameter:

$$\left\langle |\psi|^2 \right\rangle = \frac{\int |\psi|^2 \exp(-F/k_B T) d^2\psi}{\int \exp(-F/k_B T) d^2\psi} \tag{17}$$

Using the Ginzburg-Landau free energy functional $F=\int f dV$ in the Boltzmann factor of the above formula gives:

$$\left\langle |\psi_k|^2 \right\rangle = \frac{k_B T}{\alpha}(1+k^2\xi^2). \tag{18}$$

Here ξ, the Ginzburg-Landau coherence length is defined by:

$$\xi \equiv \frac{\hbar^2}{2m^*}|\alpha|^{0.5} = \frac{\xi(0)}{|\varepsilon|^{0.5}} \tag{19}$$

where again

$$\varepsilon = \frac{T - T_C}{T_C}.$$

ξ is a characteristic length scale over which local values of the order parameter ψ are correlated (at **H**=0). In order to see that, it is helpful to calculate explicitly the two-point correlation function $g(\mathbf{r},\mathbf{r}')$, where

$$g(r,r') \equiv \left\langle \psi^*(r)\psi(r') \right\rangle. \tag{20}$$

For a homogenous medium $g(\mathbf{r},\mathbf{r}')$ depends only on the relative coordinate $\mathbf{R}=\mathbf{r}-\mathbf{r}'$ and can be simplified to:

$$g(\mathbf{r})=\Sigma_k \langle|\psi_k|^2\rangle \exp(i\mathbf{k}\cdot\mathbf{R}). \tag{21}$$

Replacing the sum with an integral and carrying out the integration leads to the result:

$$g(\mathbf{R}) = \frac{m^* k_B T}{2\pi\hbar}\frac{\exp(-R/\xi(T))}{R} \tag{22}$$

Thus in the fluctuation regime in the absence of a magnetic field, spatial correlation fall off exponentially over a characteristic length scale defined by ξ.

6.1.3 Time dependent Ginzburg-Landau theory

To derive the effects of fluctuations on non-equilibrium properties such as the electrical conductivity it is necessary to use a model that includes not only time-averaged quantities such as $|\psi|^2$ but explicit time dependence. The contribution of a fluctuation to the (excess) conductivity will depend on the lifetime of the fluctuation τ, since this time will limit the period available for acceleration in an applied field. The Ginzburg-Landau theory can be extended to include time dependence.

So far, the expansion of the free energy density has been the basis for the above derivations. In the presence of gradients, currents or fields minimizing the overall free energy given by the volume integral of the equation (13) for Δf with

respect to $\psi(\mathbf{r})=|\psi(\mathbf{r})|\exp(i\phi(\mathbf{r}))$ leads to the Ginzburg-Landau differential equation:

$$\alpha\psi+\beta|\psi|^2\psi+\frac{1}{2m^*}\left(\frac{\hbar}{i}\vec{\nabla}-e^*\mathbf{A}\right)^2\psi=0 \tag{23}$$

The simplest generalization is to assume that ψ decays exponentially towards its equilibrium value (which is zero above T_C). In this case, the time dependent Ginzburg-Landau (TDGL) equation is then given by:

$$\alpha\psi+\beta|\psi|^2\psi+\frac{1}{2m^*}\left(\frac{\hbar}{i}\vec{\nabla}-e^*\mathbf{A}\right)^2\psi=-\gamma\hbar\frac{\partial}{\partial t}\psi \tag{24}$$

Neglecting the non-linear term $\beta|\psi|^2\psi$ and electromagnetic potentials gives the linearized TDGL equation:

$$\frac{\partial}{\partial t}\psi=-\frac{1}{\tau}(1-\xi^2\nabla^2)\psi \tag{25}$$

τ is the characteristic time scale of the relaxation of the k=0 mode.

The contributions of fluctuations to the conductivity that create the excess conductivity $\sigma^{fl}=\sigma_1{}^{fl}-\sigma_2{}^{fl}$ can be calculated using the ansatz

$$\sigma^{fl}=\frac{(2e)^2}{m^*}\sum_{\mathbf{k}}\frac{\left\langle|\psi_{\mathbf{k}}|^2\right\rangle\tau_k}{2} \tag{26}$$

This ansatz is motivated by analogy to the normal dc conductivity $\sigma^n=ne^2\tau_s/m$ by replacing the mean scattering time τ_s by τ and e and m by e^* and m^* respectively.

The sum over **k** can be converted into an integration depending on the dimensionality of the system. In the dc limit ($\omega=0$) σ^{fl} is given by:

$$\sigma^{fl}_{DC}\Big|_{2D} = \frac{e^2}{16\hbar d}\frac{1}{\varepsilon} \tag{27}$$

in two dimensions and by

$$\sigma^{fl}_{DC}\Big|_{3D} = \frac{e^2}{32\hbar\xi(0)}\varepsilon^{-0.5} \tag{28}$$

in three dimensions. Here d is the film thickness and $\xi(0)$ the coherence length at T=0K.

These calculations were carried out by Aslamazov and Larkin [7] and Schmidt [8,9]. They also provided the expressions for the frequency dependence of the fluctuation conductivity ($\sigma^{fl}=\sigma^{fl}{}_1-i\sigma^{fl}{}_2$) .The frequency dependence of σ^{fl} can be described by two functions $F^{\pm}{}_1(\omega\tau)$ and $F^{\pm}{}_2(\omega\tau)$:

$$\sigma^{fl}{}_1 = \sigma^{fl}_{DC}\Big|_{3D}\cdot F^{\pm}{}_1(\omega\tau) \tag{29}$$

$$\sigma^{fl}{}_2 = \sigma^{fl}_{DC}\Big|_{3D}\cdot F^{\pm}{}_2(\omega\tau) \tag{30}$$

In three dimensions $F^{+}{}_1(\omega\tau)$ and $F^{+}{}_2(\omega\tau)$ are given above T_C by:

$$F^{+}{}_{1}(\omega\tau)=\frac{8}{3(\omega\tau)^{2}}\left[1-\left(1+(\omega\tau)^{2}\right)^{\frac{3}{4}}\cos\left(\frac{3}{2}\mathrm{Arc}\tan(\omega\tau)\right)\right] \tag{31}$$

$$F^{+}{}_{2}(\omega\tau)=\frac{8}{3(\omega\tau)^{2}}\left[-\frac{3}{2}\omega\tau+\left(1+(\omega\tau)^{2}\right)^{\frac{3}{4}}\sin\left(\frac{3}{2}\mathrm{Arc}\tan(\omega\tau)\right)\right] \tag{32}$$

Below T_C, $F^{-}{}_{1}(\omega\tau)$ and $F^{-}{}_{2}(\omega\tau)$ are given above by:

$$F^{-}{}_{1}(\omega\tau)=\frac{8}{3(1+(\omega\tau)^{2})}\left[\sqrt{2}-\left(1+(\omega\tau)^{2}\right)^{-\frac{3}{4}}\left(\left(1-(\omega\tau)^{2}\right)X+2\omega\tau Y\right)\right] \tag{33}$$

$$F^{-}{}_{2}(\omega\tau)=\frac{8\omega\tau}{3(1+(\omega\tau)^{2})}\left[-\sqrt{2}+2\left(1+(\omega\tau)^{2}\right)^{-\frac{3}{4}}\left(X-\frac{\left(1-(\omega\tau)^{2}\right)}{2\omega\tau}Y\right)\right] \tag{34}$$

Where X=cos(0.5 Arctan(ωτ)) and Y=sin(0.5 Arctan(ωτ)).

In two dimensions it is also possible to write the fluctuation conductivity as a product of the dc fluctuation conductivity $\sigma^{fl}{}_{DC}|_{2D}$ and two frequency dependent functions $G^{\pm}(\omega\tau)$ [8,9]. The functions $F^{+}{}_{1}$ and $F^{+}{}_{2}$ are equal to the real and imaginary part of the 3D Gaussian scaling function [10] above T_C that is used in chapter 7 for the investigation of the scaling behavior.

In both dimensions (2D, 3D) τ, the fluctuation relaxation time is given by:

$$\tau=\frac{\pi\hbar}{16k_{B}T_{C}\varepsilon} \tag{35}$$

6.2 Temperature dependence of the dc resistivity

Before investigating the finite frequency fluctuation conductivity let us first look at the temperature dependence of the dc sheet resistance $\rho_{DC}(T)/t_0$. A plot of $\rho_{DC}(T)/t_0$ of the sample ds67a versus T is given in figure 4. Figure 5

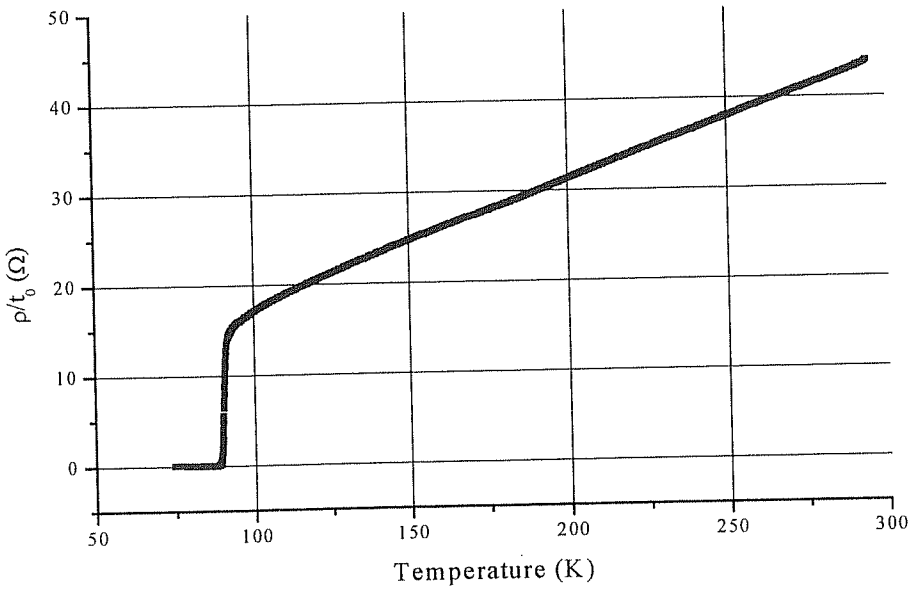

Figure 4: Plot of the dc sheet resistance ρ/t_0 of sample ds67a vs. temperature, in the temperature range 75-300K

shows the numerical derivative $d(\rho_{DC}(T)/t_0)/dT$ of the same data. Figure 5 shows that the slope is approximately constant in the temperature range from room temperature to about 20-30K above T_C. The point where the slope begins to

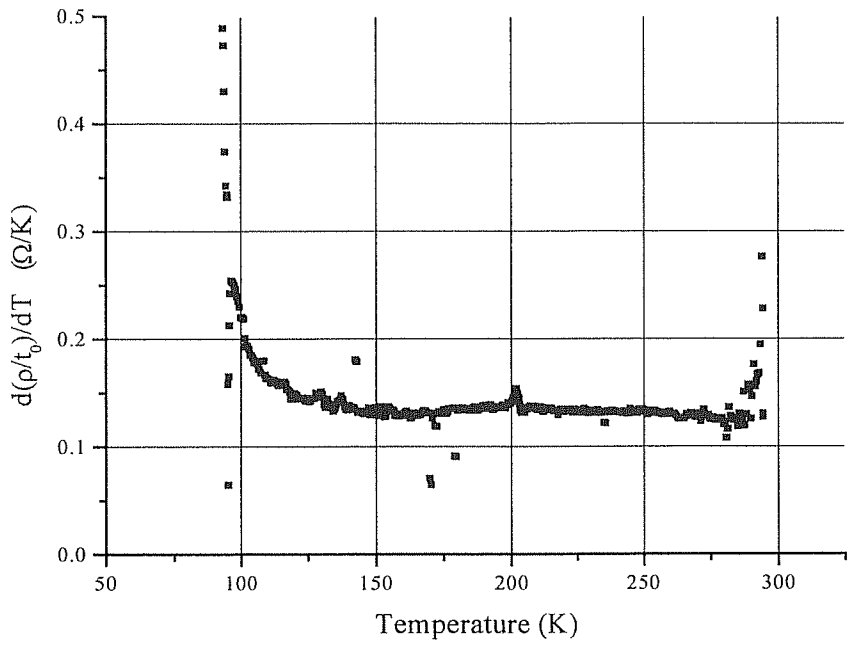

Figure 5: The numerical derivative $d(\rho/t_0)/dT$ for the sheet resistance data in figure 4.

increase is an indication for the enhanced conductivity as the temperature approaches the superconducting transition.

The dc resistivity was measured after the gold contacts were put on the film by a two-point resistance measurement between room temperature and T_C. The main purpose of this measurement is to have data to determine for the mean field normal-state conductivity.

Our measurement yields the total conductivity σ^{tot} as a function of frequency and temperature. This total conductivity σ^{tot} can be decomposed in a mean field part σ^{mf} and a contribution due to fluctuations σ^{fl}:

$$\sigma^{tot}(T,\omega)=\sigma^{mf}(T,\omega)+\sigma^{fl}(T,\omega) \tag{36}$$

To obtain the mean field conductivity we make use of the fact that the measurement is done in the microwave-range and the frequencies are much smaller than the inverse of the scattering rate. In this case σ^{mf} is frequency independent, $\sigma^{mf}(T,\omega)=\sigma^{mf}_{dc}(T)$. Empirically it is known that in the case of YBCO $\sigma^{mf}(T)=1/(\rho_0+\rho_1 T)$ for not too high temperatures in the normal state. Hence, a fit of this function combined with the appropriate model for the dc fluctuation conductivity to the normal-state resistivity data yields ρ_0 and ρ_1 as fitting parameters. Once these are known they can be used later to obtain $\sigma^{fl}(T,\omega)$, by simply subtracting $\sigma^{mf}_{dc}(T)$ from $\sigma^{tot}(T,\omega)$.

The copper oxides are characterized by a strong anisotropy and a layered structure. Therefore, it is a priori not clear, what formula should be used for the fluctuation dc fluctuation-conductivity, which depends strongly on the dimensionality of the system.

Lawrence and Doniach developed a model for the analysis of layered structures like the copper oxide materials by modeling them as system of many coupled two-dimensional superconductors [11]. The LD-model is an interpolation of the 2d and 3d forms of σ^{fl}. σ^{fl}_{LD} is given by:

$$\sigma^{fl}_{DC}\Big|_{LD}=\frac{e^2}{16\hbar d\varepsilon}\left(1+\frac{1}{\frac{1}{\varepsilon}\left(\frac{2\xi(0)}{d}\right)^2}\right)^{-\frac{1}{2}} \tag{37}$$

Here d is the inter-layer separation and $\xi(0)$ the c-axis correlation length at T=0K. The LD form of σ^{fl} contains the 2D and the 3D formulas as special cases. If the correlation length is much less then the interlayer spacing ($\xi(0) \ll d$), the fluctuation conductivity reduces to the 2D Gaussian expression, while in the opposite limit ($\xi(0) \gg d$) it recovers the three dimensional form. Further correction terms like the Maki-Thompson term in 2D that takes pair breaking effects above T_C into account are not considered in the following analysis, because they do not seem to be important at dc in low fields [12].

Figure 6 and 7 show fits to the dc sheet resistance using different models for the fluctuation conductivity and a simple mean-field behavior. A summary of the fit parameters and the fit quality is given in table 1. In the case of σ^{fl}_{2D} and σ^{fl}_{3D} four fit parameters ρ_0, ρ_1, T_C and d respectively $\xi(0)$ are used. The Lawrence-Doniach model requires five parameters ρ_0, ρ_1, T_C, d and $\xi(0)$. In the first row of table 1 we give the result of a purely mean field fit without taking fluctuations into account ($\sigma^{fl}=0$), leading to only three fitting parameters ρ_0, ρ_1 and T_C.

Fit	ρ_0 ($\mu\Omega$cm)	ρ_1 ($\mu\Omega$cm/K)	T_C (K)	ξ_0 (Å)	d(Å)	Fit range (K)	Fit quality (χ^2)
Mf	70.47	1.99	-	-	-	149-280	$0.695*10^{-14}$
2-D	70.17	2.02	90.14	-	8.82	90.69-280	$3.97*10^{-14}$
3-D	54.94	2.10	90.67	2.49	-	90.69-280	$45*10^{-14}$
LD	78.16	2.05	90.57	6.08	18.45	90.69-280	$3.15*10^{-14}$

Table 1: Fitting parameters to the dc resistance vs. temperature data. The fit quality is in Ω/degrees of freedom and a minimum for the best fit

Note: The fit quality of the mean-filed fit and the fits to fluctuation conductivity can not be directly compared to each other, because of the different fitting ranges. The Lawrence-Doniach model gives the best fit of the three models of the fluctuation conductivity, with the fitting parameters for the mean field resistivity ρ_0=78.16μΩcm and ρ_1=1.99μΩcm.

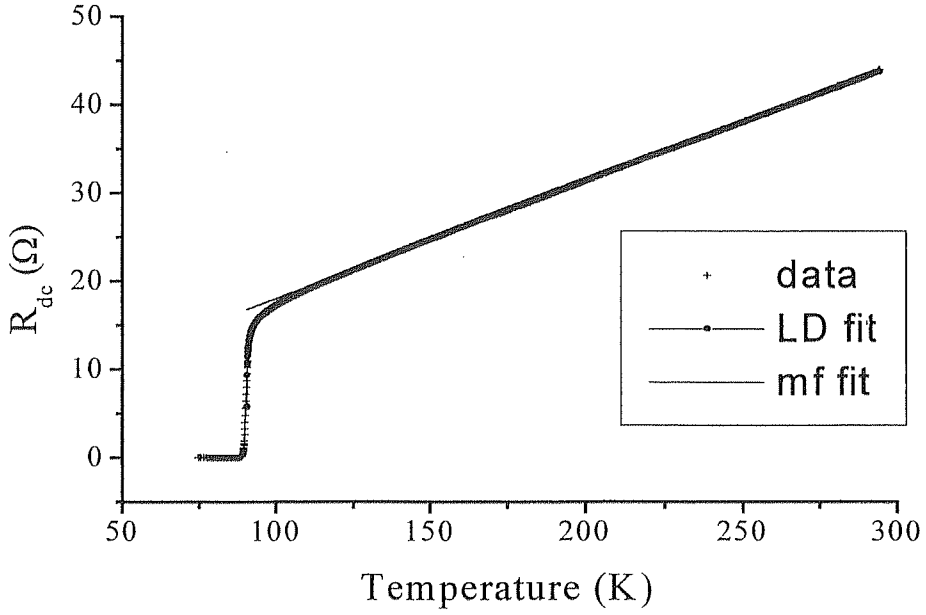

Figure 6: The Lawrence-Doniach (line with circles) and mean-field (solid line) fits to the dc sheet resistance.

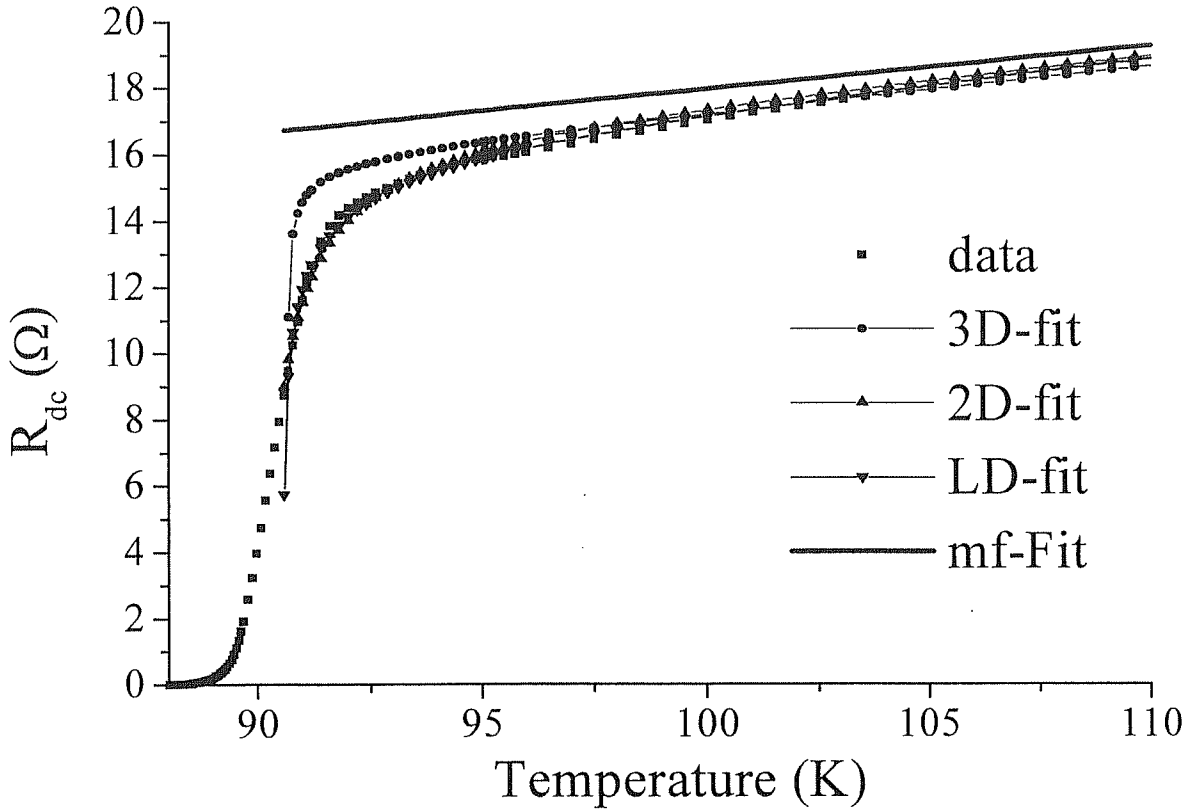

Figure 7: Fits to the dc sheet resistance vs. temperature using different models of the fluctuation conductivity near T_C.

Chapter 7: Scaling Theories

Very close to T_C fluctuation effects dominate the transition; they are no longer small. In this critical region, the derivation of the Gaussian fluctuation conductivity is no longer valid, since non-linear and higher order terms cannot be neglected. In addition, the expansion of the free energy density in terms of the assumed to be small order parameter ψ breaks down. In this region a more general scaling theory [1,2] is needed. A brief description of such a theory that can be used to obtain expressions for the fluctuation conductivity in the critical region is given in this section.

The general scaling theories assume that the coherence length ξ as well as the fluctuation relaxation time τ are symmetric around T_C and diverge at T_C:

$$\xi(T) = \frac{\xi_0}{|\varepsilon|^{\nu}} \tag{38}$$

Where $\varepsilon=(T-T_C)/T$. ξ_0 is a non- universal sample-dependent length. The exponent ν is not restricted to $\nu=1/2$ as in the Gaussian theory but can take any positive value.

The relaxation time τ scales as $\tau \sim \xi^z$, where z is the dynamical critical exponent. Thus,

$$\tau = \frac{\tau_0}{|\varepsilon|^{\nu z}} \tag{39}$$

τ_0 is a non-universal time scale that depends on the specific sample.

Combining this with the assumption that the conductivity below T_C is proportional to the superfluid density ρ_s ($\rho_s \sim \xi^{2-d}$) makes it possible to describe the scaling of the conductivity σ. The constraint that σ should remain finite as $T \rightarrow T_C$ leads to the following form for the (low-frequency) conductivity:

$$\sigma(T,\omega) \approx \xi^{2-d+z} S_{\pm}(\omega\tau) \tag{40}$$

where $S_{\pm}(\omega\tau)$ are universal scaling functions above (S_+) and below (S_-) T_C, z is the dynamical critical exponent and d the dimensionality of the system. It is especially useful to look at the scaling behavior of the phase angle ϕ_σ,defined by $\sigma = |\sigma| \exp(i\phi_\sigma)$. The phase should scale near the transition as:

$$\phi_\sigma(T,\omega) = \Phi_{\pm}(\omega\tau) \tag{41}$$

where in analogy to $S_{\pm}(\omega\tau)$, $\Phi_{\pm}(\omega\tau)$ are universal scaling functions that do not depend on the individual sample-dependent parameters T_C, τ_0 and ξ_0.

In the limit $T=T_C$, $S_{\pm}(\omega\tau)$ and $\Phi_{\pm}(\omega\tau)$ simplify significantly. Since ξ^{2-D+z} diverges at T_C, but σ should stay finite at the same time, the magnitude of the conductivity must scale as:

$$|\sigma(T = T_C, \omega)| = c|\omega|^{-(2-D+z)/z} \tag{42}$$

The phase ϕ_σ on the other hand is, for a given z and dimensionality D, a constant independent of frequency at $T=T_C$:

$$\phi_\sigma(T = T_C, \omega) = \frac{\pi}{2}\left(\frac{2-D+z}{z}\right) \tag{43}$$

The limiting forms of the scaling functions are especially useful to pinpoint T_C by investigating the curves of the isotherms of the magnitude $|\sigma^{fl}|$ and phase of the fluctuation conductivity. However, explicit forms of the complex scaling function $S_+(\omega\tau)$ also exist, calculated by Wickham and Dorsey [3]:

$$S_+(\omega\tau) = \frac{2z^2}{(D-2+z)(D-2)(\omega\tau)^2}\left[1 - \frac{D-2+z}{z}i\omega\tau - (1-i\omega\tau)^{(D-2+z)/z}\right] \tag{44}$$

This form of the scaling function S_+ includes the Gaussian form of the scaling function as a special case for z=2. The Gaussian form of S_+ has been calculated earlier by Dorsey [2] and the resulting fluctuation conductivity agrees with the corresponding formulas in chapter 6. The scaling function for the phase of σ is $\Phi_+(\omega\tau)$ and is given by:

$$\Phi_{+}(\omega\tau) = \text{Arc}\tan\frac{\text{Im}(S_{+}(\omega\tau))}{\text{Re}(S_{+}(\omega\tau))} \tag{45}$$

$$= \text{Arc}\tan\left(\frac{\omega\tau\left(D-2+z\right)}{z\left(\left(D-2+(\omega\tau)^2\right)^{\frac{D-2+z}{z}}-1\right)}\right)$$

Chapter 8: Data and Analysis

8.1 The complex resistivity near T_C

The main advantage of the Corbino reflection geometry is the ability to measure the complex resistivity $\rho(T,\omega)=\rho_1(T,\omega)+i\rho_2(T,\omega)$ over a wide range of frequencies in the microwave range. Figure 8 shows the temperature dependence of the real part of the sheet resistance of sample ds67a, (the resistivity ρ_1 divided by the film-thickness t_0) at a number of different measurement frequencies.

At high temperatures, in the normal state, ρ_1 appears to be frequency independent; the data at all frequencies fall on the same curve. This behavior is a consequence of the fact that the normal state scattering rate ($1/\tau_n$) is much larger than the measurement frequencies over the entire frequency range [1]. However, as the temperature is lowered and the system enters the region of the superconducting transition, the data show more and more frequency dependence. In fact, the transition appears to broaden as the measurement frequency increases. At even lower temperatures, below the transition temperature, the frequency dependence becomes weaker again and the values of ρ_1/t_0 become very small [2].

The temperature dependence of the imaginary part of the sheet resistance, ρ_2/t_0, is shown in figure 9 at the same measurement frequencies as figure 8. The main feature of the temperature dependent data is a peak that grows as the

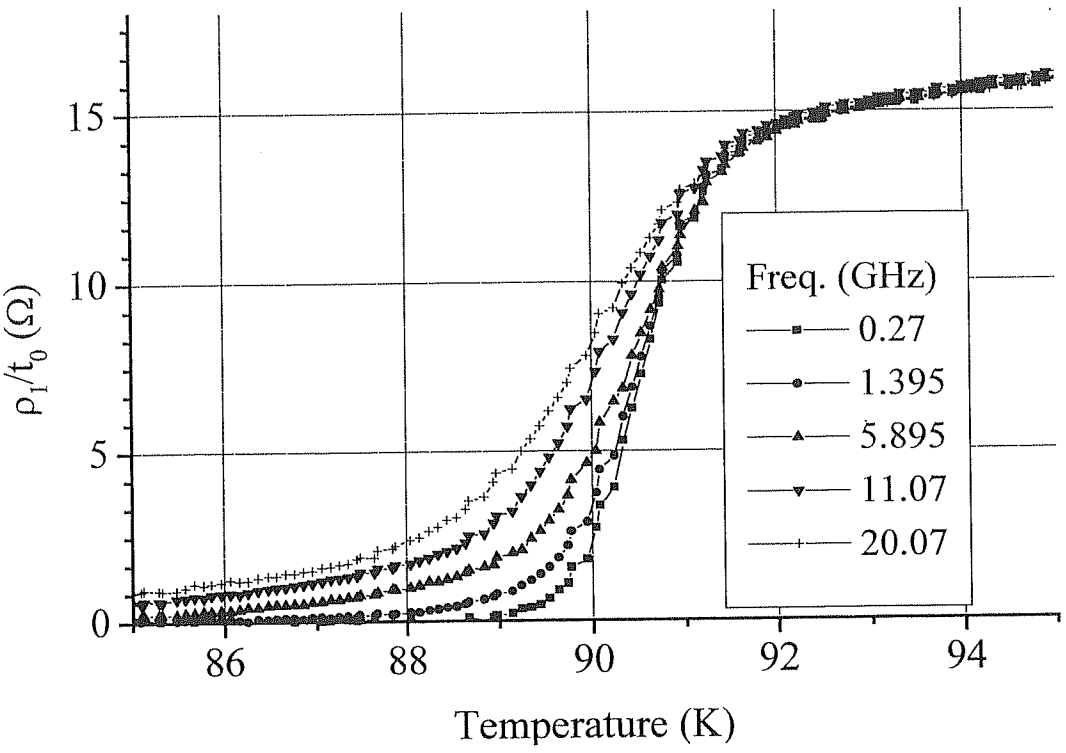

Figure 8: Real part of the sheet resistance vs. temperature at different frequencies

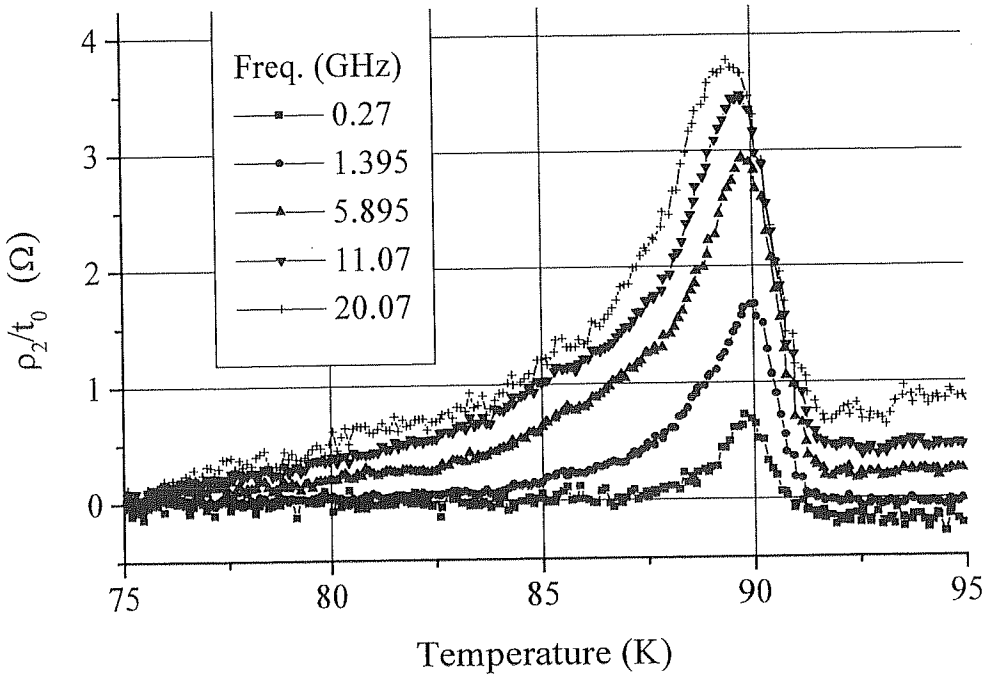

Figure 9: Imaginary part of the sheet resistance vs. temperature at different frequencies

measurement frequency increases. The position of this peak is temperature dependent and moves to lower temperatures for higher frequencies. The fall off of ρ_2/t_0 at temperatures well below T_C is a result of the temperature dependence of the microwave penetration depth λ, since $\rho_2/t_0 \approx \mu_0\omega\lambda^2(T)/t_0$ for T sufficiently below T_C [3]. Above the transition temperature ρ should be completely real since, as pointed out before, the measurement frequencies are much lower than the normal state scattering rate [1]. The fact that ρ_2/t_0 in figure 9 seems to be a constant non-zero value at high frequencies is an artifact of an inadequate correction procedure.

The Corbino reflection technique is a swept-frequency measurement that yields not only the temperature dependence but also the frequency dependence of the complex resistivity. The frequency dependence of ρ_1/t_0 and ρ_2/t_0 at several temperatures in the vicinity of T_C is shown in the next two figures 10 and 11. Figure 10 shows ρ_1/t_0 over the entire measurement frequency range (45MHz-45GHz) at different temperatures. At high temperatures above the transition temperature ρ_1/t_0 is approximately frequency independent. In the transition region ρ_1/t_0 exhibits some frequency dependence and becomes very small well below T_C.

ρ_2/t_0 versus frequency at the same temperatures as is shown in fig(11). As with ρ_1/t_0,it shows some frequency dependence in the midst of the transition region. At lower temperatures, well below T_C, again $\rho_2/t_0 \approx \mu_0\omega\lambda^2(T)/t_0$ is valid,

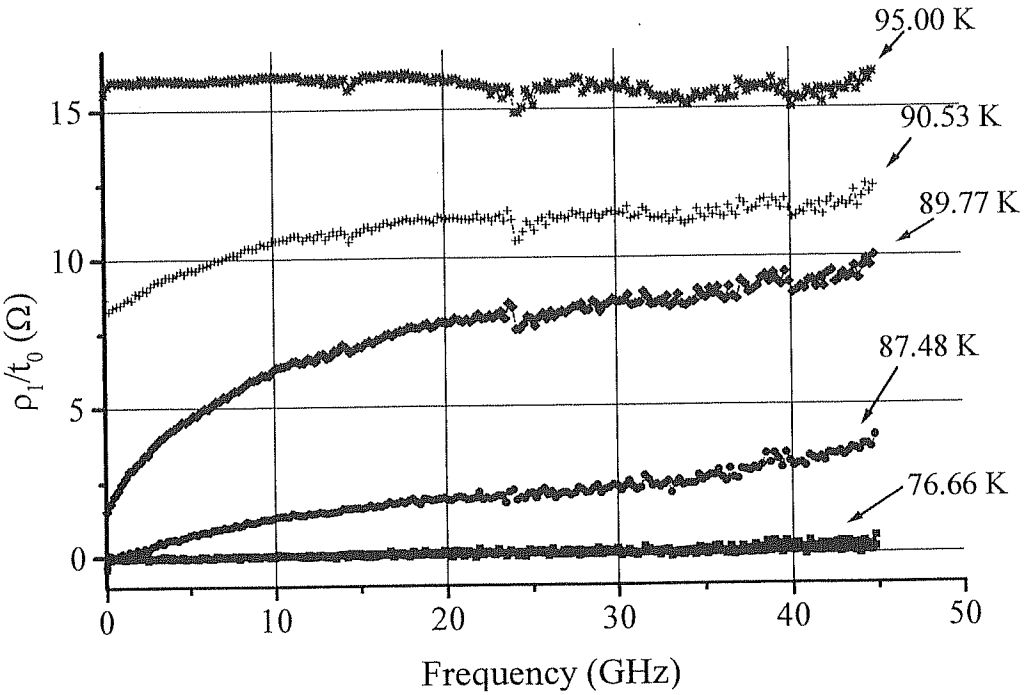

Figure 10: Real part of the sheet resistance versus frequency at temperatures near Tc. T_C=89.94K is determined in section 8.2.

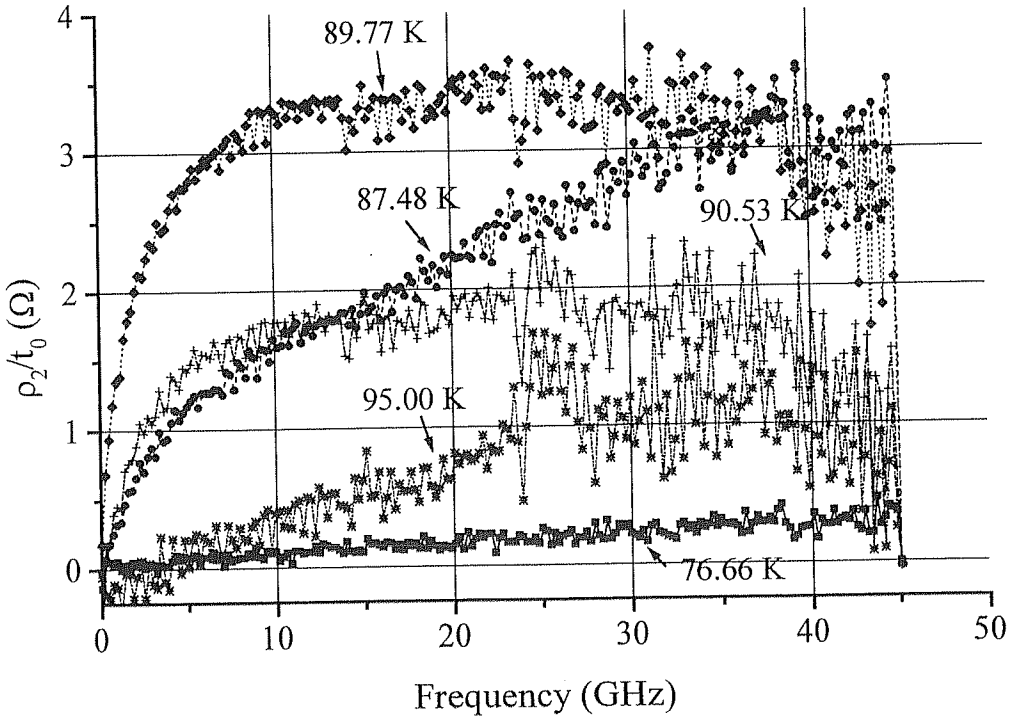

Figure 11: Imaginary part of the sheet resistance versus frequency at temperatures near Tc. T_C=89.94K is determined in section 8.2.

resulting in a roughly linear frequency dependence of $\rho_2(\omega)$. Above T_C ρ_2/t_0 seems to be non-zero and very noisy, which is due to the same problem in the calibration procedure that was mentioned already above in the discussion of the temperature dependence.

8.2 Fluctuation effects in the frequency dependent conductivity

To investigate the scaling behavior it is convenient to convert the frequency dependent data of the measured complex resistivity to a conductivity σ. The conductivity data can then be regarded as the sum of a fluctuation part σ^{fl} and a mean-field contribution σ^{mf}. To investigate the frequency dependence of the fluctuation conductivity, the mean field contribution as determined from the dc resistivity fits is first removed.

Once the fluctuation conductivity is obtained the frequency dependence of the fluctuation conductivity magnitude ($|\sigma^{fl}|=[(\sigma^{fl}{}_1)^2+(\sigma^{fl}{}_2)^2]^{1/2}$) and phase $\phi_\sigma=\mathrm{Arctan}[\sigma^{fl}{}_2/\sigma^{fl}{}_1]$ can be compared to the predictions of scaling theory discussed in chapter 7. An important role is played by the frequency dependence at $T=T_C$. According to scaling theory, the phase angle of the fluctuation conductivity should take on a frequency-independent constant value at the critical temperature T_C. This value depends only on the dimensionality D of the system and the critical exponent z: $\phi_\sigma(T=T_C,\omega)=(\pi/2)(2\text{-}D+z)/z$ [4].

The corresponding frequency dependence of the magnitude of the fluctuation conductivity is a power law behavior at the critical temperature: $|\sigma^{fl}(T=T_C,\omega)|=c\ \omega^{-\alpha}$, with $\alpha=(2-D+z)/z$. The investigation of the frequency dependence of isotherms of the phase and magnitude of the fluctuation conductivity can therefore be used to obtain a value for the dynamical critical exponent z provided that the dimensionality D is known.

Figures 12 and 13 show the measured frequency dependence of the magnitude and phase of the fluctuation conductivity at temperatures in the vicinity of T_C. The critical isotherm in the frequency dependence of the magnitude of the fluctuation conductivity is determined by fitting a power law behavior to all measured isotherms and comparing the quality of the fits. In this manner we found the best fit to the $|\sigma^{fl}|$-data at T=88.94K. As can be seen from figure 13 the phase of the fluctuation conductivity takes on a roughly constant value at T=88.94K. Hence the behavior of magnitude and phase is consistent and it is reasonable to define the isotherm at T=88.94K as the critical isotherm. In addition the behavior of the phase of the fluctuation conductivity is even more convincing if the concavity of the isotherms is taken into account. The isotherms of the phase below T_C bend up at low frequencies, where the isotherms above T_C bend down. The critical isotherms separate these two regions clearly. The data sets are taken at 0.1K intervals therefore there is some uncertainty in the exact determination of T_C from the frequency dependence of the conductivity. Certainly, T_C lies at least between the temperatures of the adjacent isotherms

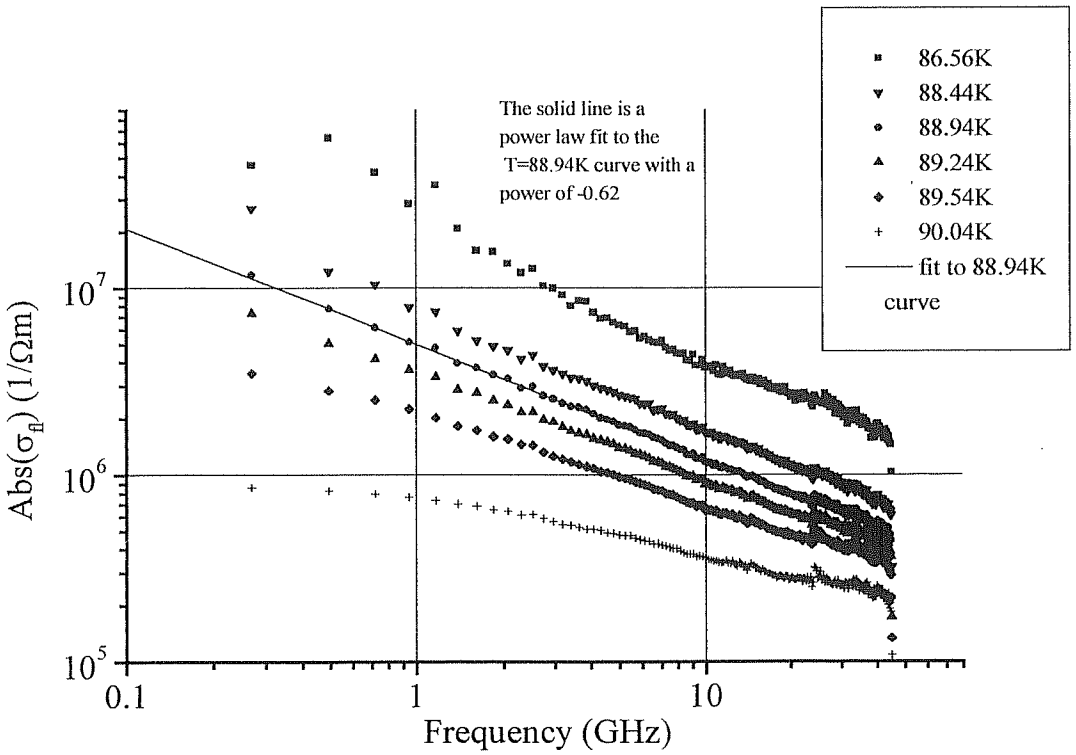

Figure 12: Magnitude of the fluctuation conductivity near Tc

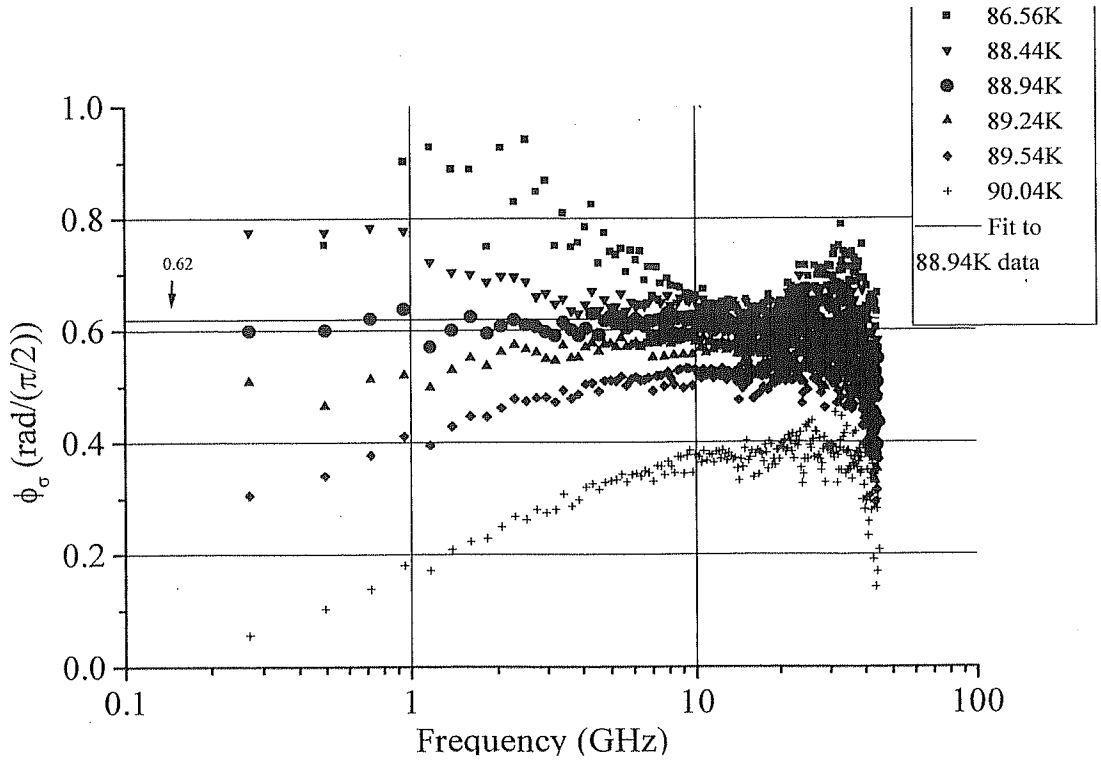

Figure 13: Reduced phase of the fluctuation conductivity near Tc. The solid line is a constant value of 0.62

meaning that we get T_C=(88.94±0.1)K. In any case the uncertainty in T_C affects the exact determination of the critical phase angle and power law values. The fitting parameters are also not completely independent of the fitting range. Fitting the isotherms of the phase instead of the magnitude however give, as expected, only slightly different results.

Fitting the frequency dependence of the magnitude of the fluctuation conductivity with $|\sigma^{fl}| \propto \omega^{-\alpha}$ at T=(88.94±0.1)K yields α=0.60-0.63 for the fitting range 0.4-10GHz and α=0.60-0.64 for the fitting range 0.4-20GHz. The data at higher frequencies seems to be much noisier, especially in the phase, and therefore is not taken into account here. Fits to the phase of the fluctuation conductivity at T=(88.94±0.1)K with $\phi=(\pi/2)\alpha$ yield α=0.59-0.63 for the fitting range 0.4-10GHz and for the fitting range 0.4-20GHz. Taking the lowest and highest value that was obtained for α, we get α=0.59-0.64. Since $\alpha=(2-D+z)/z$ the value of the dynamical critical exponent lies in the range z=2.44-2.78 if we assume the dimensionality of the system D=3. This assumption is justified because the size of the fluctuations, the coherence length ξ, diverges as T approaches T_C, so even an apparently two-dimensional, layered system will eventually become three-dimensional. The results for the value of the critical exponent z are larger than the prediction in Gaussian theory of z=2. This suggests critical behavior in the sample.

Note that the values that we obtained for T_C and z stay the same within the stated range for the different values of the mean field contribution that were obtained by fitting functions from different models (2D,3D, Lawrence-Doniach) to the normal state resistivity.

8.3 Scaling of the frequency dependent conductivity above T_C

The value of the critical exponent $z \approx 2.6$ that we obtained in the previous section can be used to investigate the scaling behavior of the frequency dependent fluctuation conductivity σ^{fl} at temperatures above and below T_C. In this section, the scaling behavior of σ^{fl} is investigated. From scaling theory it is expected that the fluctuation conductivity scales with the appropriate power of the correlation length ξ and the fluctuation lifetime τ^{fl} as can be seen from the following equation (40) from chapter 7 [4]:

$$\left|\sigma(T = T_C, \omega)\right| = c\left|\omega\right|^{-(2-d+z)/z} \qquad (40)$$

The functions S_+ and S_- are scaling functions above (S_+) and below (S_-) T_C. S_+ and S_- are universal and equal for all members of a given universality class as should be the critical exponents ν and z. equation (40) combined with the assumptions D=3, $\xi(T) \sim \varepsilon^{-\nu}$ and $\tau \sim \xi^z$ implies that the quantity $\sigma^{fl}(T,\omega)\varepsilon^{\nu(z-1)}$ plotted versus the scaled frequency $\omega\varepsilon^{-\nu z}$ yields the universal scaling function $S_{\pm}$. To determine if the measured data really shows scaling behavior, we plot the scaled conductivity measured at different temperatures versus the scaled

frequency. From scaling theory the parameters T_C, ν and z are undetermined and can be chosen such that the data sets all collapse onto the same universal curve. However, we have fixed already the transition temperature T_C to be T_C=(88.94±0.1)K and the critical exponent z to be z≈2.6 by investigating the behavior of the critical conductivity isotherm. Only the value of ν is yet undetermined and can be adjusted to collapse the data.

Figure 14 shows the scaled fluctuation conductivity versus the scaled frequency that collapses onto a single curve with ν chosen to be ν=2.2. The other

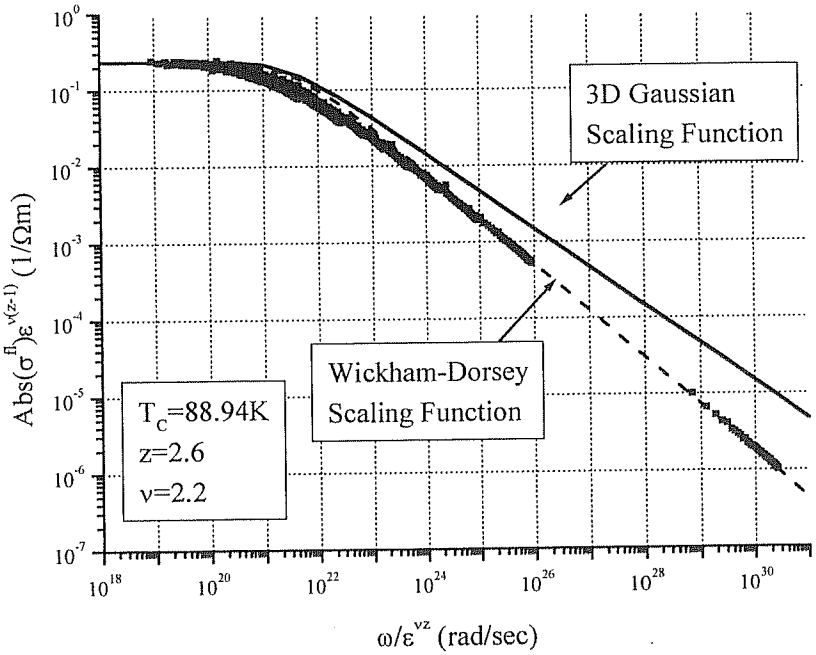

Figure 14: Scaling behavior of the phase of the fluctuation conductivity and theoretical curves: 3D Gaussian scaling function (solid line) and WD Scaling function (dashed line). Shown is data above T_C in the range T=88.97-90.7K and f=0.27-10GHz.

parameters are T_C=88.94K and z=2.6.

Shown are data above T_C in a range of roughly 1.8K. Also shown is the 3D Gaussian scaling function [4] which incorporates z=2 and the more general Wickham-Dorsey scaling function [5] that is valid for general values of z. The Wickham-Dorsey function shown in figure 14 was calculated using the experimentally determined value of z=2.6. The data is in good agreement with the Wickham-Dorsey form of the scaling function and differs significantly from the Gaussian prediction for large arguments. The limit where the argument is very large corresponds to temperatures very close to T_C. In this limit, the 3D Gaussian scaling function approaches a power law of -0.5, while the data and the Wickham-Dorsey scaling function approach a power law of -0.62.

Like the magnitude of the fluctuation conductivity, it is also possible to investigate the behavior of the phase of the fluctuation conductivity, which should scale as $\phi_\sigma(T,\omega)=\Phi_\pm(\omega\tau)$. Figure 15 shows a plot of the measured conductivity phase angles versus the scaled frequency $\omega\tau$ using the same values for T_C, z, ν that were used to scale the magnitude of the fluctuation conductivity. Figure 15 shows also plots of the phase angel of the 3D Gaussian scaling function and the Wickham-Dorsey form. The data clearly approaches a constant value of roughly 0.62. It is in good agreement with the Wickham-Dorsey scaling function while the 3D Gaussian scaling function shows a similar functional dependence, but reaches a maximum value of 0.5 for large argument.

The scaling behavior of the fluctuation conductivity above as well as below T_C is shown in the next two figures (figure 16 and 17). The temperature

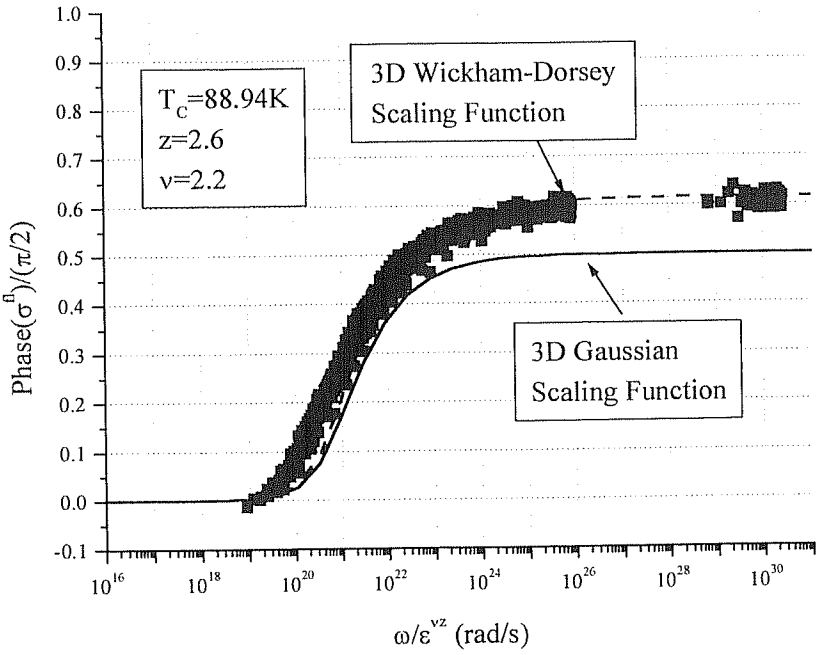

Figure 15: Scaling behavior of the phase of the fluctuation conductivity and theoretical curves: 3D Gaussian scaling function (solid line) and WD Scaling function (dashed line). Shown is data above T_C in the range T=88.97-90.7K and f=0.27-10GHz.

range of the data in these figures is 87.88-91.46K, while the values of T_C, ν and z are the same as in the previous figures. One can clearly see that the data for temperatures above and below T_C collapse onto two curves that take on the same form in the limit of large argument.

The frequency dependent data clearly shows scaling behavior in both the

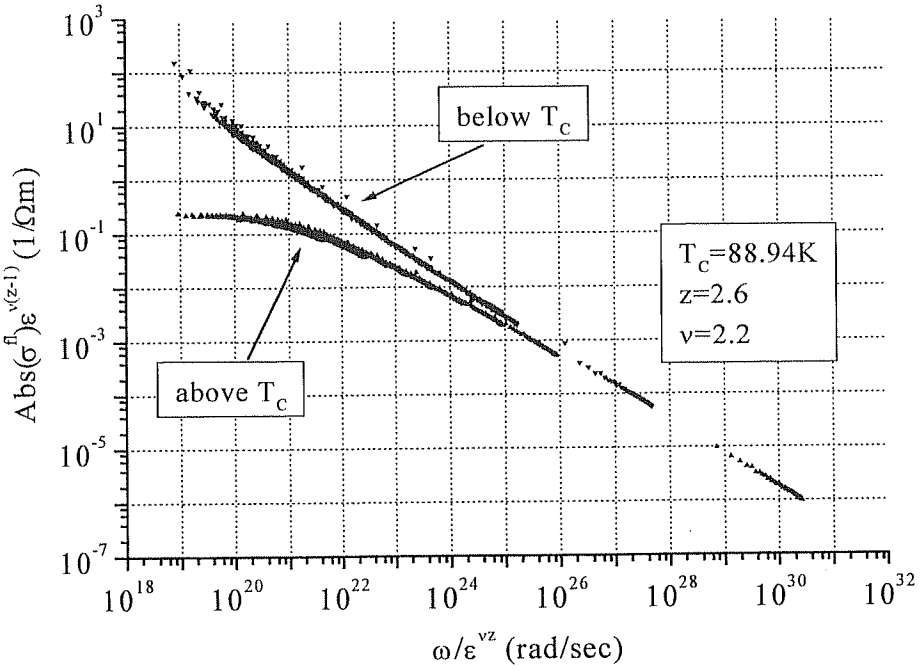

Figure 16: Scaling behavior of the magnitude of the fluctuation conductivity above and below T_C. Shown is data in the temperature range 87.15-88.84K below and 88.98-90.73K above T_C

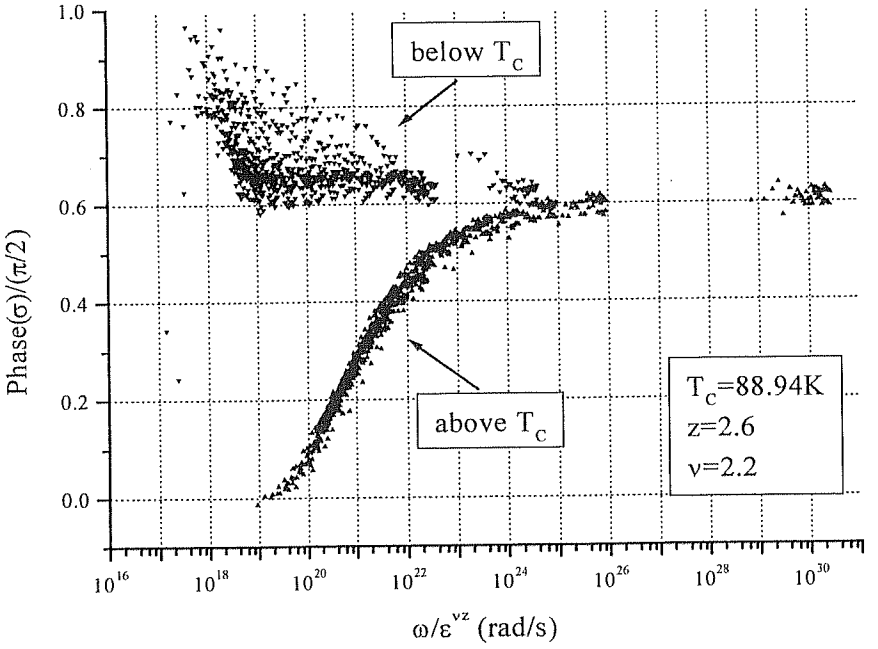

Figure 17: Scaling behavior of the phase of the fluctuation conductivity above and below T_C. Shown is data in the temperature range 87.15-88.84K below and 88.98-90.73K above T_C

magnitude and phase of the measured fluctuation conductivity with the same values for the critical exponents ν=2.2, z=2.6, T_C=88.9K. However, it should be noted that the data shows scaling behavior over a range of values for ν. Scaling behavior can be reached for values of ν between 1.5 and 3.5. An example for the scaling behavior of the data with a different value of ν that lies in that range is shown in the figures 18 and 19.

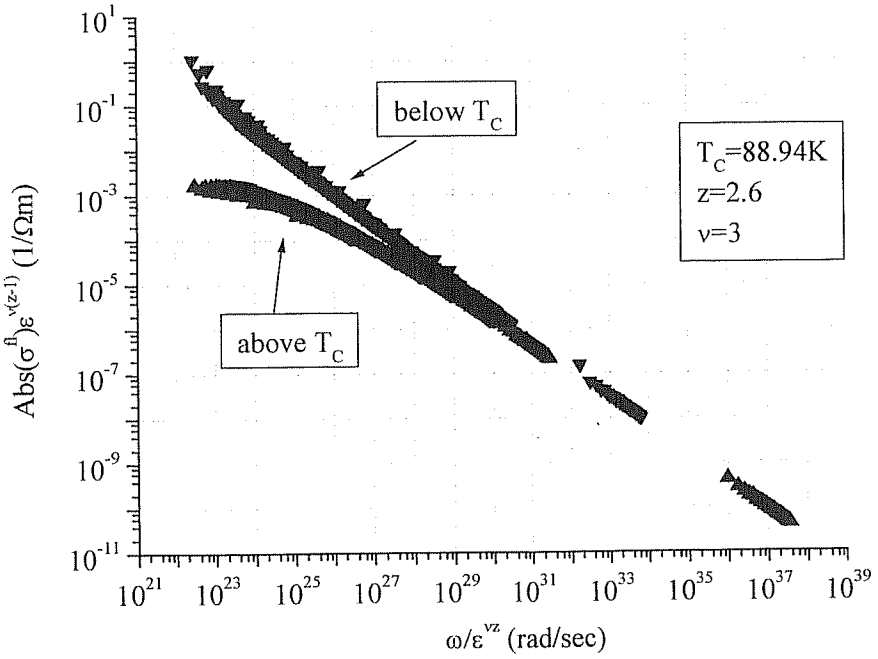

Figure 18: Scaling behavior of the magnitude of the fluctuation conductivity above and below T_C. Shown is data in the temperature range 87.15-88.84K below and 88.98-90.73K above T_C

Here ν is chosen to be ν=3. With this value for ν both the magnitude and the phase of the fluctuation conductivity the data can also be collapsed onto two curves, one above and one below T_C.

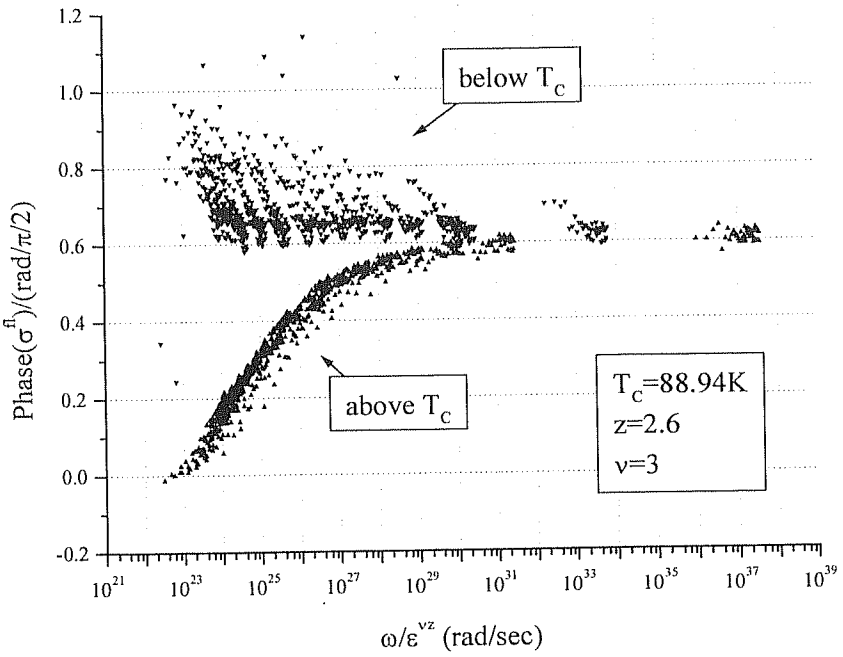

Figure 19: Scaling behavior of the phase of the fluctuation conductivity with $\nu=3$.

However, although there is some ambiguity in the exact value of ν, we find no data collapse for $\nu=1/2$, the value that is predicated by the Gaussian theory. Figure 20 and figure 21 show the attempt to reach a data collapse of the data with $\nu=1/2$ for the magnitude and phase of σ^{fl}. The other parameters T_C and z are not changed. The data collapse is not as clear as in the previous figures (16-19) and indicates that the reasonable values of ν are larger than 1/2.

In spite of the uncertainty in the exact values of the critical exponents, ν as well as z, it can be concluded that the fluctuation lifetime $\tau^{fl} \propto \varepsilon^{-\nu z}$ diverges faster than the Gaussian prediction of $\tau^{fl} \propto \varepsilon^{-1}$ as T approaches T_C. This is also shown in the next section.

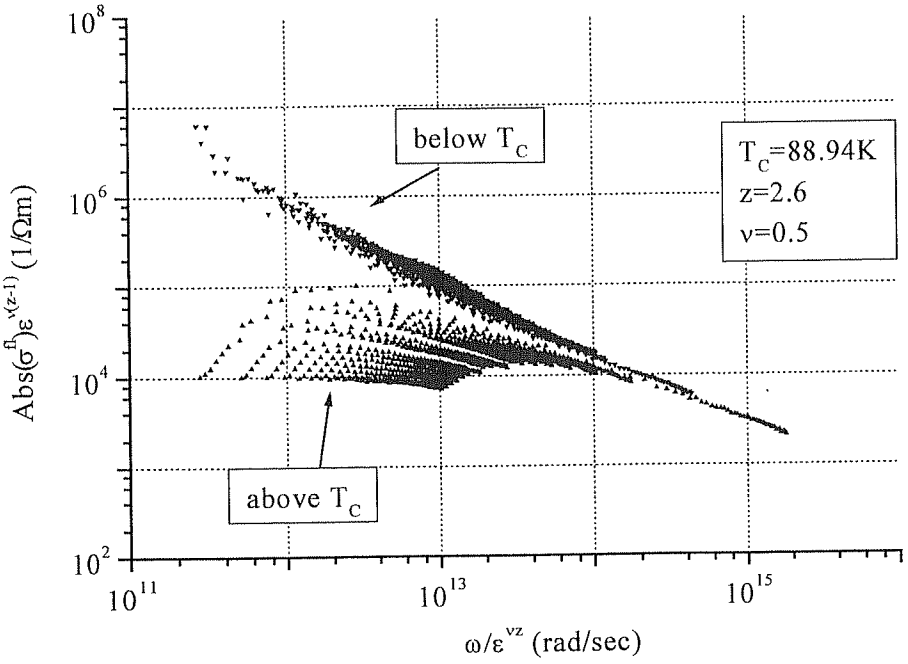

Figure 20: Scaling behavior of the magnitude of the fluctuation conductivity with ν=0.5 as predicted by Gaussian theory

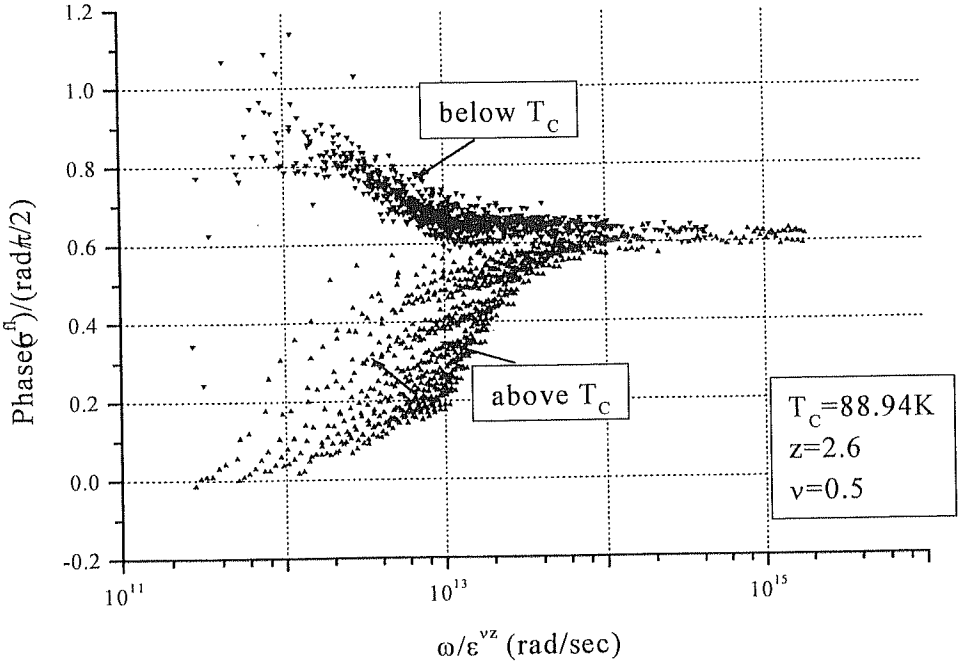

Figure 21: Scaling behavior of the phase of the fluctuation conductivity with ν=0.5 as predicted by Gaussian theory

8.4 Further investigation of the scaling below T_C

We have shown in section 8.3. that the scaling of the conductivity data above T_C is in good agreement with theoretical expressions. Unfortunately, there is no theoretical expression for the scaling function below T_C available, but we can start to investigate the scaling below T_C by comparing it to expressions derived from Gaussian theory. The scaled magnitude of the conductivity data is shown in figures 16 and 18: the data above and below T_C clearly collapse onto two curves, which lay on top of each other for large arguments. In this limit, at temperatures close to T_C, the data shows a power-law behavior with the same power above and below T_C. At temperatures further away from T_C the curves split. The data above T_C goes to a limiting value for small $\omega\tau$, which is in agreement with the theoretical forms of the scaling functions. Below T_C the data does not seem to saturate but appears to diverge. This behavior in the limits of large and small $\omega\tau$ is in agreement with a prediction of the behavior of the scaling function below T_C (S^-) by Fisher, Fisher and Huse [6]. According to this prediction S^- should behave as $S^- \sim i/(\omega\tau)$ for $\omega\tau \to 0$, which eventually recovers the behavior of the conductivity of a superconductor as described by the two-fluid model [7]. This prediction implies that the phase of the conductivity goes to $\pi/2$ in the limit of small $\omega\tau$, which seems to be consistent with the behavior of the data shown in figures 17 and 19.

In the absence of a theoretical expression for S^- another approach is to check if the behavior of the data can be qualitatively described by the frequency dependent functions $F_1^-(\omega\tau)$ and $F_2^-(\omega\tau)$ that were found by Schmidt [8] (equations 33 and 34) in analogy with the situation above T_C. A plot of magnitude and phase of $F^-=F_1^-+iF_2^-$ and as a comparison F^+ versus $\omega\tau$ is shown in figures 22 and 23.

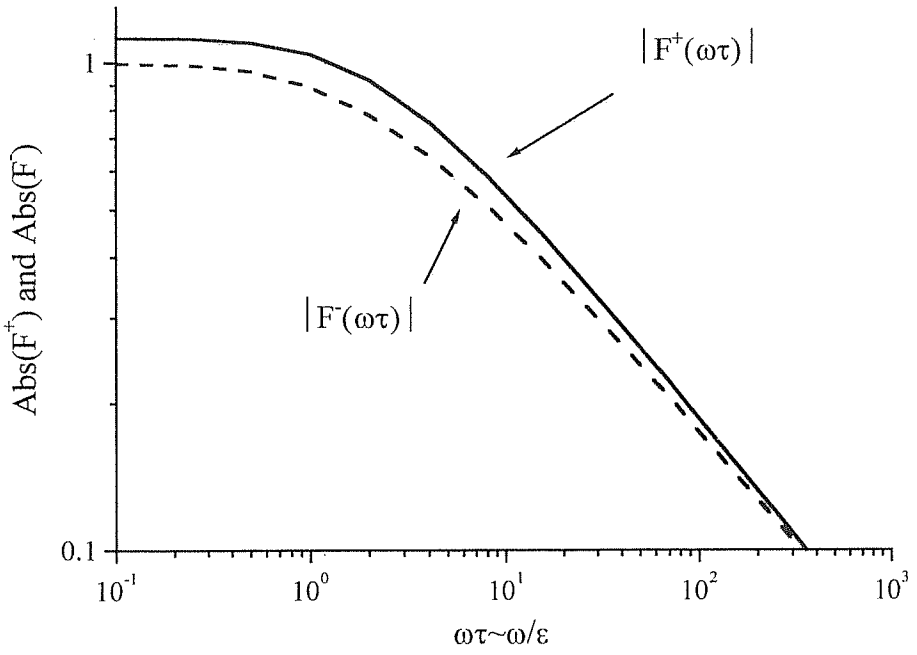

Figure 22: Magnitude of the frequency dependent function F^+ (straight line) and F^-(dashed line) vs. $\omega\tau$

F^+ and F^- show a similar behavior in magnitude and phase. The magnitude of both functions has a power law behavior for large $\omega\tau$ and goes to a finite value for $\omega\tau\rightarrow 0$. The behavior of the scaled phases $\Phi(F^+)$ and $\Phi(F^-)$, which

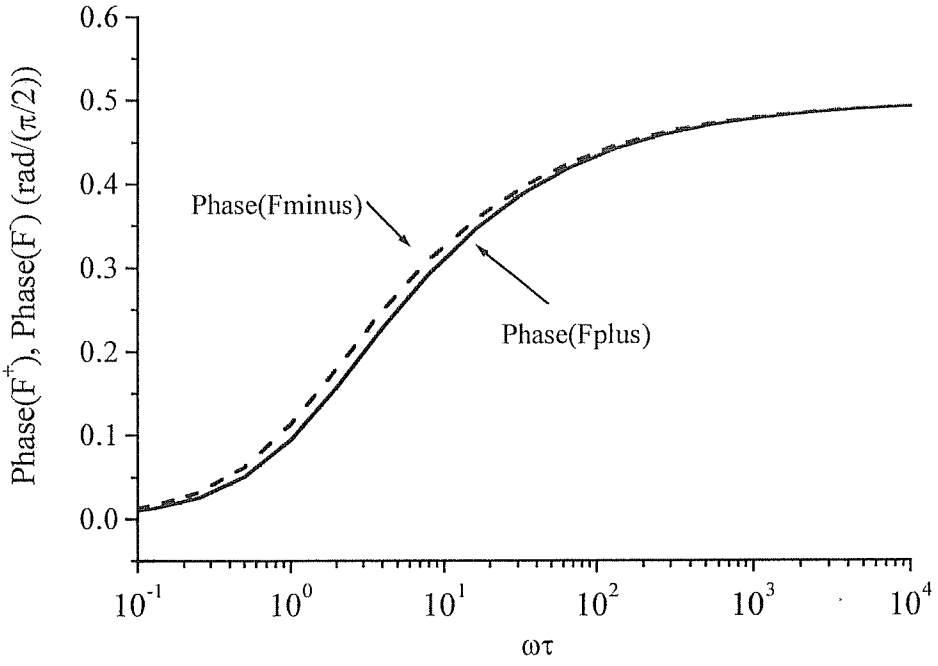

Figure 23: Phase of the frequency dependent functions F^+ (straight line) and F^-(dashed line) vs. $\omega\tau$

go both to 1/2 as $\omega\tau\rightarrow\infty$ and to 0 for $\omega\tau\rightarrow\infty$ are similar. Clearly, F^- does not describe the behavior of the data shown in figures 16-19. The reason for this might be that F^- was derived for the fluctuation conductivity only, whereas the data contains the total conductivity with only the mean-field contribution above T_C removed. In the following, I want to describe preliminary results of the attempt to find and subtract off the mean field part of the conductivity below T_C. This treatment is by no means complete and should only be regarded as a "first step".

To describe the mean-field conductivity below T_C we can use expressions derived from BCS-theory [9]:

$$\sigma^{mf}(T,\omega) = \sigma_1^{BCS}(T,\omega) - i\sigma_2^{BCS}(T,\omega) \tag{41}$$

As a start we concentrate only on the imaginary part of the mean-field conductivity and leave out the real part completely, because the imaginary part of σ^{mf} is much larger than its real part just below T_C [7]. The imaginary part of the mean field conductivity σ_2^{BCS} is given by:

$$\sigma_2^{BCS} = \frac{\pi\Delta(T)}{\hbar\omega}\tanh\left(\frac{\Delta(T)}{2k_BT}\right)\cdot\sigma^{NS}(T) \tag{42}$$

$\Delta(T)$ is the temperature dependence gap energy and $\sigma^{NS}(T)$ is equal to the dc normal state conductivity extended to temperatures below T_C. The gap energy close to T_C is given by:

$$\Delta(T) = 1.74\sqrt{\frac{T_C - T}{T_C}}\Delta(0) \qquad T\approx T_C \tag{43}$$

where

$$\Delta(0) = 1.764 * k_B T_C \tag{44}$$

is the zero temperature gap energy.

A fit of of σ_2^{BCS}, with an additional factor in equation (43) as a fitting parameter, to the temperature dependent σ_2-data at the frequency f=2.295GHz is shown in

figure 24. The plot shows clearly that the data is much larger than zero at temperatures close to T_C and above, whereas the BCS-fit goes to zero as $T \rightarrow T_C$.

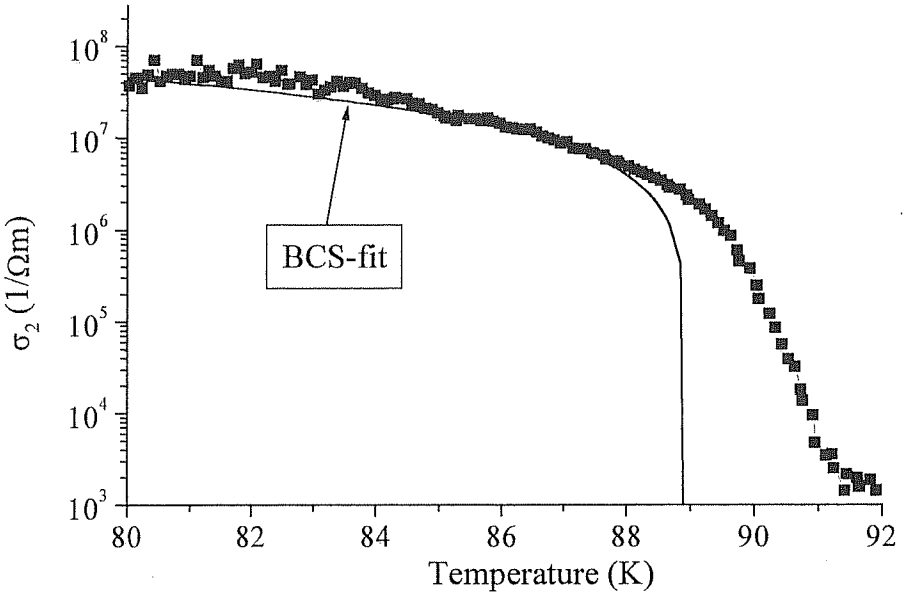

Figure 24: σ_2 data at f=2.295GHZ and BCS-fit below T_C

The difference between the curves, shown in figure 25 is the fluctuation σ_2, which peaks around T_C. Figure 25 also shows two fits to the fluctuation σ_2^{fl} using the Schmidt expressions (equations 29 and 30) for the imaginary part of the fluctuation conductivity.

To remove the mean-field conductivity at all measured frequencies we use the BCS expression combined with the fitting parameter determined by the fit in figure 25. This corrected data together with the corresponding $\sigma_1(T,\omega)$ gives the fluctuation conductivity σ^{fl} below T_C. The scaling behavior of the

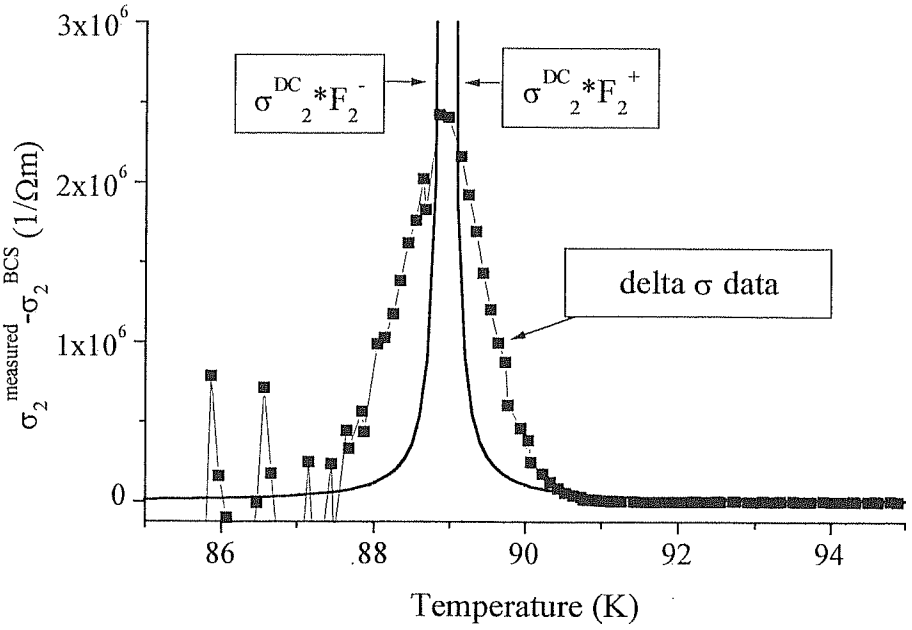

Figure 25: Difference between measured σ_2 and BCS expression σ_2^{BCS}

magnitude and phase of σ^{fl} corrected this way is shown in figure 26 and 27. The figures also show the uncorrected data and the behavior of magnitude and phase of F^-. Figure 26 shows that for large $\omega\tau$ the corrected and uncorrected data have power law behavior, whereas it is not clear whether or not the corrected data will saturate as $\omega\tau \rightarrow 0$ as suggested by the behavior of F^-. The changes in the phase (figure 27) are more dramatic. Before the correction the scaled phase seemed to flat or even go up for small $\omega\tau$, whereas the phase of the corrected data clearly goes to zero in that limit, in qualitative agreement with the behavior of the phase

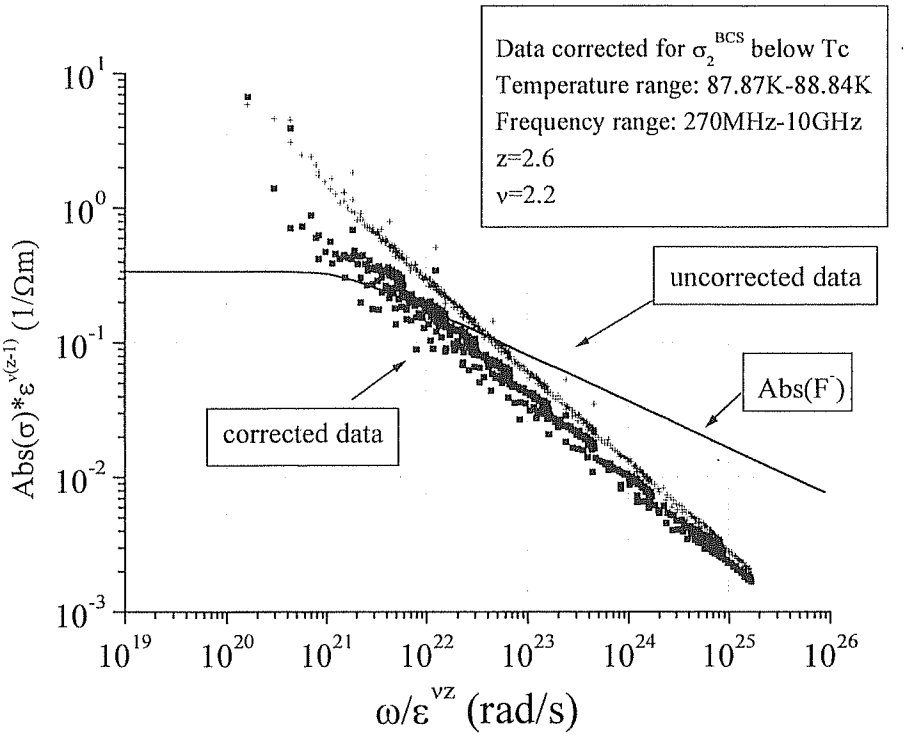

Figure 26: Comparison of the scaling behavior of the magnitude of the corrected (squares) and uncorrected (crosses) data

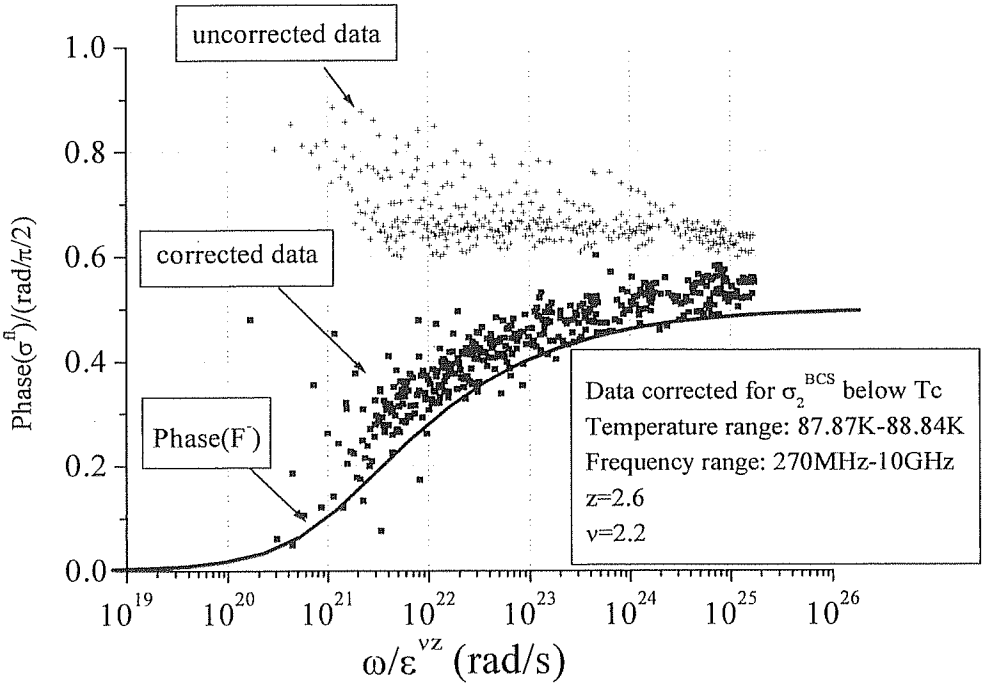

Figure 27: Comparison of the scaling behavior of the phase of the corrected (squares) and uncorrected (crosses) data

of F". For large $\omega\tau$ the scaled phase of corrected and uncorrected data goes to a fixed value around 0.6.

Figure 26 and 27 show that at least qualitatively the scaling behavior of the fluctuation conductivity in magnitude and especially in phase agree with the behavior of F". It is possible that this agreement would further increase with the appropriate correction of the data for σ_1^{mf} that was omitted here.

8.5 Temperature dependence of the fluctuation conductivity

Figure 22 shows a plot of the real part of the fluctuation conductivity σ_1^{fl} versus the reduced temperature $\varepsilon=(T-T_C)/T_C$ at several fixed frequencies. To calculate ε we used a value of T_C=88.94K as determined from the critical scaling. As can be seen from the figure for each frequency curve there is one specific temperature where it splits off from the other curves. This is an indication of the fact that the fluctuation relaxation rate $1/\tau^{fl}$ passes through the measurement frequency. In the dc limit, the fluctuation conductivity diverges as $\varepsilon\rightarrow 0$. However, for finite frequencies the fluctuation lifetime τ^{fl} remains finite. This causes a cut off in the divergence when $\omega\sim 1/\tau^{fl}$. The points were this cut off occurs for the shown measurement frequencies are indicated by arrows in the figure; at these points, frequency and fluctuation relaxation rate are of the same order, $\omega\tau^{fl}\sim 1$. In other words at large values for ε ($\varepsilon>2*10^{-2}$) all frequency curves lay on top of each other, because $\omega\tau^{fl}<<1$ leads to a frequency independent σ_1^{fl}.

At values for ε that correspond to $\omega\tau^{fl}\sim1$, the data becomes frequency dependent and the curves split (indicated by the arrows). If ε is decreased even further (closer to T_C) we have the situation where $\omega\tau^{fl}>1$. In this case σ_1^{fl} is frequency dependent, the frequency curves remain apart and show strong frequency dependence. According to Gaussian theory the curves should remain together until $\varepsilon\sim10^{-3}$ for the measurement frequencies. This is a further indication that the sample shows critical behavior close to T_C.

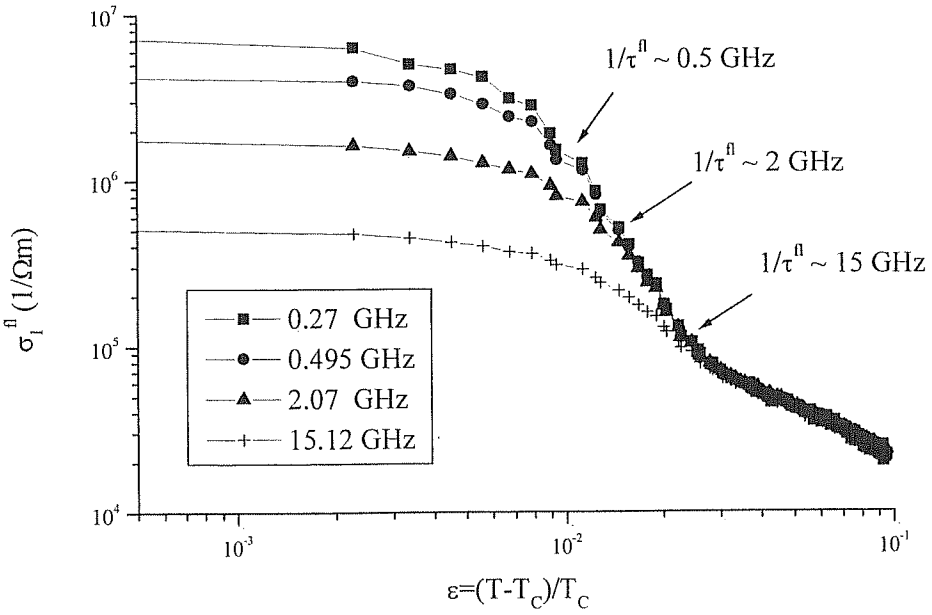

Figure 28: Plot of the fluctuation conductivity σ^1 vs. ε at different frequencies. The arrows indicate roughly the points where the curves split, because $1/\tau^{fl}$ is equal to the measurement frequency

Chapter 9: Conclusions and Future Work

9.1 Review of results and conclusions

We have successfully measured the surface impedance of $YBa_2Cu_3O_{7-\delta}$ thin films in the microwave frequency range of 45MHz-45GHz at temperatures around the transition temperature. From the surface impedance data we were able to extract the complex conductivity and investigate fluctuation effects near T_C. We find that at a specific temperature the enhanced conductivity due to fluctuations has a frequency dependence that is consistent with the predictions of general scaling theory: a pure power law dependence of the magnitude and a frequency independent behavior of the phase of the fluctuation conductivity. We have used this behavior to locate the thermodynamic critical temperature of the sample and to measure the dynamical critical exponent z. We found that z lies in the range 2.44-2.78. This is larger than the prediction of z=2 of the Gaussian theory, which is an extension of Ginzburg-Landau theory. We also investigated the scaling behavior of the fluctuation conductivity around T_C and find that both magnitude and phase of the fluctuation conductivity can be collapsed onto universal curves. We investigated this for data above and below the thermodynamical critical temperature and find that the data collapses on two curves above and below T_C that fall together in the limit were $T \rightarrow T_C$. Above T_C the scaling behavior of magnitude and phase are in good agreement with the

Wickham-Dorsey scaling function that generalizes the Gaussian scaling function if the experimentally determined value of z is used. The investigation of the scaling behavior yields also values for the critical exponent ν. We have found values for ν in the range of ν=1.5-3.5 that are larger than the value of the Gaussian prediction of ν=1/2. Our values of ν and z indicate that the fluctuation lifetime $\tau^{fl} \sim \varepsilon^{-\nu z}$ diverges quicker than in Gaussian theory (where νz=1) in the critical region close to T_C.

9.2 Future Experiments

The Corbino apparatus has shown that it can be successfully used to investigate fluctuation effects in $YBa_2Cu_3O_7$. It would be fruitful to go to other high T_C superconducting materials to investigate the scaling behavior and the universality of the critical exponents. We have improved the existing experimental set up so that it can be reliably used for measurements at lower temperatures. Measurements with $Pr_{1.85}Ce_{0.15}Cu_4O$ (PCCO) have so far yielded preliminary results. We have reached the temperature region of the superconducting transition of PCCO but we have not been able to cool the PCCO-samples far enough below their transition temperature. For the investigation of fluctuation effects PCCO is an interesting material, because it belongs to the high T_C materials, but is more 'two-dimensional' than YBCO, which should result in larger fluctuation effects. The main future improvement that could lead to the possibility to reach lower temperatures is probably to use a

longer coaxial cable. In addition, the cooling from the cold finger to the sample could be improved by redesigning the attachment of the copper barrel that holds the coaxial cable.

REFERENCES

Chapter 1

[1] J. G. Bednorz and K.A. Müller, Z. Phys. B 64, 189 (1986)

[2] Heat capacity N. Overend et al., Phys. Rev. Lett. 72, 3238 (1994)

[3] S. Kamal et al., Phys. Rev. Lett. 73, 1845 (1994)

[4] A. Schwartz, M. Scheffler and S.M. Anlage, Phys. Rev. B **61**, 870,(2000)

[5] D.R. Strachan, C.J. Lobb, unpublished

[6] Charalambous et al., Phys. Rev. Lett. 83, 2042,(1999)

[7] J. Booth et al., Phys. Rev. Lett. 77, 4438 (1996)

[8] J. Booth, Ph.D. dissertation, University of Maryland 1996

[9] A description of the original apparatus can be found in: J.C. Booth, D.H. Wu, S.M. Anlage, Rev.Sci. Instrum 65(6), (1994)

Chapter 3

[1] The load impedance is in general the impedance of whatever is at the end of the coaxial cable. $Z_{load}=V_{tot}/I_{tot}$ neglects any effects due to the electrical contact R_{cont} between cable and sample. To minimize this contact resistance gold contacts are evaporated on the sample. If R_{cont} is too large than the load impedance is simply dominated by contacts effects and the measurement is not sensitive to the sample at all.

[2] The impedance transformation is only valid with the assumption that the substrate is semi-infinite. This is obviously not the case. In fact, Z_{sub} is later regarded as an effective substrate impedance that takes effects due to resonances in the substrate into account.

[3] The equation $\rho_2=\mu_0\omega\lambda^2(T)$ can be derived from the two-fluid model, with the assumption $\omega\tau_n \ll 1$, where τ_n is the normal electron scattering rate. The two-fluid model describes the electrodynamics of a superconductor from the superposition of the response of "superconducting" and "normalconducting" electron fluids. It is described in many textbooks, see for example: M. Tinkham, "Introduction to Superconductivity", Second Edition, McGraw-Hill, New York, (1996), chapter 2.

Chapter 4

[1] D. H. Wu, J. C. Booth, and S. M. Anlage, Phys. Rev. Lett. **75**, 525 (1995)

[2] J. C. Booth et al., Phys. Rev. Lett. 77, 4438, (1996)

[3] A. Schwartz, M. Scheffler, S.M. Anlage, Phys. Rev. B, **61** (2000)

[4] "Pulsed Laser Deposition of thin Films", K. Hubler and D.B. Chrisey, Eds., John Wiley and Sons, New York (1994)

Chapter 5

[1] A description of the calibration procedure can also be found in:
Student guide for Basic Network Measurements using the HP8510B Network Analyzer System Edition 3.0 (1988)

[2] The assumption of the frequency independence of the resistivity ρ is true if $\omega\tau \ll 1$, (Hagen-Rubens limit)- where $1/\tau$ is the scattering rate. At the microwave frequencies, where this measurement is done this is always the case.

Chapter 6

[1] C. J. Lobb, Phys. Rev. B **36**, 3930 (1987)

[2] A thin film must have a thickness of the order of the size of the fluctuations ξ for this to be true.

[3] J. Booth, Ph.D. dissertation, University of Maryland 1996

[4] M. Tinkham, "Introduction to superconductivity", Second Edition, McGraw-Hill, Inc., New York (1996), chapter 4

[5] "High Temperature Superconductivity", J. W. Lynn, Ed, Springer-Verlag, New York (1990)

[6] W. J. Skocpol and M. Tinkham, Rep. Prog. Phys., **38**, 1049 (1975)

[7] L.G. Aslamov and A.I. Larkin, Sov. Phys. Solid State, **10**, 875, (1968)

[8] H. Schmidt, Z. Phys., **216**, 336, (1968)

[9] H. Schmidt, Z. Phys., **232**, (443), 1970

[10] A.T. Dorsey, Phys. Rev. B **43**, 7575, (1991)

[11] W. E. Lawrence and S. Doniach, Proceedings of the Twelfth International Conference on Low-Temperature Physics, Kyoto 1970, edited by E. Kanda, (Keigaku, Tokyo, 1970), p.361

[12] W. Liu, T.W. Clinton, A.W. Smith and C.J. Lobb, Phys. Rev B **55**, (11802) (1997)

Chapter 7

[1] D. S. Fisher, M. P. A. Fisher, D. A. Huse, Phys. Rev. **B 43**, 130, (1991)

[2] A. T. Dorsey, Phys. Rev. B **43**, 7575 (1991)

[3] R. A. Wickham and A. T. Dorsey, cond-mat/9906124 9June1999

Chapter 8

[1] In the normal state the frequency dependence of the conductivity can be expressed by the Drude formula $\sigma=\sigma_n^{dc}/(1+i\omega\tau_n)$, where σ_n^{dc} is the normal dc conductivity. In our measurements we have always $\omega\tau_n \ll 1$, which leads to a conductivity and therefore to a resistivity $\rho=1/\sigma$ that is frequency independent.

[2] In fact $\rho_1(T=75K,\omega)\equiv 0$ was assumed in order to be able to correct the room-temperature calibration for temperature dependent changes (see 5.2.).

[3] The equation $\rho_2=\mu_0\omega\lambda^2(T)$ can be derived from the two-fluid model, with the assumption $\omega\tau_n \ll 1$, where τ_n is the normal electron scattering rate. The two-fluid model describes the electrodynamics of a superconductor from the superposition of the response of "superconducting" and "normalconducting" electron fluids. It is described in many textbooks, see for example: M. Tinkham, "Introduction to Superconductivity", Second Edition, McGraw-Hill, New York, (1996), chapter 2.

[4] A. T. Dorsey, Phys. Rev. B **43**, 7575 (1991)

[5] R. A. Wickham and A.T. Dorsey, cond-mat/9906124 9June1999

[6] D.S. Fisher,M.P.A. Fisher, D.A. Huse, Phys. Rev. B **43**, 130,(1991)

[7] From two-fluid model: $\sigma_2 \sim (1/\omega)$ and $\sigma_2 \gg \sigma_1$ for $\omega \neq 0$. For derivations see for example: Tinkham, "Introduction to Superconductivity", Second Edition, McGraw-Hill, New York, (1996), Chapter 2

[8] H. Schmidt, Z. Phys. **232**, (443), 1970

[9] BCS theory is for example described in: Tinkham, "Introduction to Superconductivity", Second Edition, McGraw-Hill, New York, (1996), Chapter 3